ABSTRACT

Title of Thesis: LAMINAR SMOKE POINTS OF COFLOWING DIFFUSION FLAMES IN MICROGRAVITY

Thomas F. DeBold, Master of Science, 2012

Directed By: Dr. Peter Sunderland, Associate Professor
Department of Fire Protection Engineering

Nonbuoyant laminar jet diffusion flames in coflowing air were observed aboard the International Space Station with an emphasis on laminar smoke points. The tests extended the 2009 Smoke Points In Coflow Experiment (SPICE) experiment to new fuels and burner diameters. Smoke points were found for methane, ethane, ethylene, and propane burning in air. Conditions included burner diameters of 0.76, 1.6, 2.1, and 3.2 mm and coflow velocities of 3.0 – 47 cm/s. This study yielded 57 new smoke points to increase the total number of smoke points observed to 112. Smoke point lengths were found to scale with burner diameter raised to the -0.67 power times coflow velocity raised to the 0.27 power. Sooting propensity was observed to rank according to methane < ethane < ethylene < propane < 50% propylene < 75% propylene < propylene. This agrees with past normal gravity measurements except for the exchanged positions of ethylene and propane. This is the first time a laminar smoke point has been observed for methane at atmospheric pressure.

LAMINAR SMOKE POINTS OF COFLOWING DIFFUSION FLAMES IN MICROGRAVITY

By

Thomas Francis DeBold

Thesis submitted to the Faculty of the Graduate School of the
University of Maryland, College Park in partial fulfillment
of the requirements for the degree of
Master of Science
2012.

Advisory Committee:
Associate Professor Dr. Peter B. Sunderland, Chair
Associate Professor Dr. André Marshall
Associate Professor Dr. Arnaud Trouvé
Special Member Dr. David L. Urban

Acknowledgements

This work was done in conjunction with NASA as a part of the Smoke Points In Coflow Experiment (SPICE). The coordinating contact for the project was Dr. David L. Urban. The experiments were done in the International Space Station by astronaut Don Pettit and directed by Dr. Urban. The experiments were funded through NASA. This thesis was advised by Dr. Sunderland. My contribution was through data collection and analysis.

There are many people I would like to thank for contributions to this project as well as contributions to my education at the University of Maryland. First, I would like to thank Dr. Peter Sunderland for bringing me onto this project in my switch to a research Masters degree from the professional Masters degree. I used Dr. Sunderland's level of knowledge on the combustion process throughout my thesis. His passion for research work helped me through the compressed time frame that I had for my research. I would also like to specially thank Dr. Urban of NASA, my coordinating contact on the project. Dr. Urban worked with myself and Dr. Sunderland at our weekly meeting and provided guidance and knowledge on my research. Without Dr. Urban I would not know some of the subtleties of the SPICE project necessary for writing my thesis.

I would like to thank the Department of Fire Protection for their dedication to spreading their knowledge of fire and fire protection engineering. The learning environment I was put into is a great contributor to my success as a student. Dr. Milke's figure in the fire protection community inspired me to continue my education. The whole department was always willing to help any student that sought it. Pat Baker not only

helped me coordinate my defense but went above and beyond in helping with my transition from the M.E. program to the M.S. program.

I'd like to thank the Keystone department for the financial support. Working with Dr. Hines has been a great experience and has helped fuel a passion for teaching. I got experience in front of a classroom that will without doubt help me in my future endeavors.

I'd like to thank Chas Guy for his help in editing this paper. His expertise in English helped me through the task of proofreading this paper. He helped me make sure the following project was as clear as possible to the reader. Lastly, I'd like to thank my parents, friends, and my family for helping me through the toughest parts of my final semester. Without all of the support, my completion would have been much more difficult.

Table of Contents

List of Figures and Tables

Chapter 1: Introduction

Soot is a topic in the fire and combustion research that is important yet not completely understood. Incomplete combustion causes the production of soot. Radiation from soot is what causes the human eye to see flame as a bright yellow to dull orange color [1]. It can provide the light and warmth for which people build fires. However, soot radiation also causes increases in heat loads and contributes to fire spread rates. Fire spread rates are increased from radiation from the soot and can shorten the Available Safe Egress Time (ASET) in fire situations. Increase in heat loads from radiation is particularly a problem with engines because radiation can cause a loss in efficiency and unexpected temperatures. Radiation heat losses in a conventional diesel engine are around 1.1% of the total fuel energy [2]. In many fire situations soot radiation contributes more than gaseous radiation to heat transfer [3]. Soot has significant adverse health effects in long term and short term exposures [4]. Soot emissions correlate with carbon monoxide, which is a major cause of death in fires [5]. Climate change and glacier melting have been linked with soot concentrations at high elevations [6]. Soot is an important topic in fire phenomena and continued research in soot formation can lead to a better understanding of predicting and eventually controlling soot production.

1.1 Smoke Points

Laminar smoke points are the generally used measure of fuel sooting tendency in diffusion flames. The laminar smoke point of the flame is the condition where the flame

is non sooting but is at the threshold of producing soot. Any increase in fuel flow rate will cause the flame to emit soot [7]. Laminar smoke point properties are usually measured from round buoyant jet diffusion flames with coflowing air. The length of the flame at the smoke point is the indicator of the flames tendency to soot. A longer smoke point length is a characteristic of a flame that produces less soot. Smoke points have been measured for gaseous, liquid, and solid fuels. Currently there is ASTM1322 "Standard Test Method for Smoke Point of Kerosene and Aviation Turbine Fuels," but this standard applies to wick fed liquid fuels and not gas jet fuels. Smoke points of gaseous fuels are found from a coflowing jet flame apparatus with excess of oxygen. Gaseous fuels have been studied under normal gravity systems [8] as well as under elevated pressures [9] to help understand flame systems. Testing smoke points under elevated pressures is especially useful for combustion devices and gas turbines. Not only for the function of the device, but also for the environmental concerns of fuel emissions [9].

There are four commonly used explanations for the occurrence of smoke points that are not mutually exclusive[10]. The first is a smoke point occurs when the soot temperature reaches its critical temperature of 1300 K (1000 K for microgravity) before its burnout [10, 11, 12]. Another explanation of smoke point is that the radiative loss fraction increases until it reaches 0.2-0.4 for normal gravity or 0.4-0.6 for microgravity with the increase of fuel flow rate [10, 13, 14, 15, 16, 17, 18]. The ratio of the luminous length and the stoichiometric length increase with increased fuel flow until it reaches a smoke point around two [10, 16, 19, 20]. Lastly the increase in flame residence time also increases the time available for soot formation and oxidation. Longer residence

times can increase radiative loss fractions and the volume of radiating soot [10, 21]. Figure 1.1 shows a smoke point condition for an ethylene flame.

In normal gravity, laminar smoke points have been found to correlate with soot volume fractions and radiative loss fractions of turbulent diffusion flames. This connection is important for understanding the smoke production in turbulent flames. Flames that have a longer laminar smoke point will have a lower soot formation rate. Shorter smoke points indicate greater soot formation rates. The relationship between a fuel's peak soot formation rate and its laminar smoke point is being used for CFD calculation of fire radiation [22]. Turbulent flow conditions are harder to model, but are more useful in fire simulations.

Figure 1.1: Ethylene sooting flame

1.2 Soot Formation

Understanding the sooting tendencies of hydrocarbon fuels relative to one another is important for the highly desired control of the fuels soot production. The tendency of

a flame to produce soot is strongly related to the type of flame, combustion process, and other physical parameters. It is important to recognize that all of these factors contribute to the flames tendency to soot. The fuels that have been tested in this study are non-aromatic hydrocarbon fuels. Non-aromatic fuels undergoing a pure or oxidative pyrolysis will form aromatic rings during combustion. Moss (1995) and Leung (1991) simplified the formation of soot to four main mechanisms: nucleation, heterogeneous surface growth, coagulation, and oxidation [23, 24, 25]. During the combustion process aromatic rings are formed to create polycyclic aromatic hydrocarbons (PAHs). Hydrocarbons with simple structures like methane are more difficult to thermally decompose than a more complex hydrocarbon like ethylene [9]. In the thermal decomposition acetylene is formed and combines to form benzene rings. Those benzene rings form together to make PAHs. PAHs are products of incomplete combustion and are precursors to soot formation [26]. These particles grow and eventually form into particle nuclei when large enough. The growing particles coagulate increasing the size of the particles. PAHs levels have been found to be higher in under ventilated fires that produce more smoke. Once soot is formed, it needs time to oxidize in the upper parts of the flame [22]. As the soot travels through the flame it is cooled to a point where it can no longer be oxidized [23]. Soot formation and oxidation increase as temperature increases, but oxidation rate increases faster with temperature.

Soot formation processes are different based on the structure of the process taking place. It is important to understand the structure of the process, whether it be premixed, coflowing flames, inverse coflowing flames, counter flowing diffusion flames, or shock tubes. Buoyancy effects also need to be considered. Santoro studies of soot formation

in coannular diffusion flames showed that a characteristic of smoking flames were "wings" or "horns" around the sides of the flame [34, 44]. These characteristic horns were caused by intense nucleation and agglomeration in the toroidal zone near the base. The soot formed in this toroidal zone is convected along streamlines towards the tip of the flame. The horns are formed around the outside of the flame because of these streamlines of soot. From Kent and Wagner's [10, 27] research on soot temperatures, flames start emitting soot when the soot temperature in the oxidation zone cools below 1300 K with the effects of buoyancy. Nonbuoyant flames were found by Urban [10, 28] to have temperatures of 1000 K when a smoke point condition was reached. The decrease in temperature for nonbuoyant flames is the result of radiative quenching because of the increased residence times of nonbuoyant diffusion flames.

The most extensive work on sooting of laminar diffusion flames done by Schalla [29, 40] showed that the sooting tendency decreases in the followed order: Aromatics > Alkynes > Alkenes > Alkanes. Aromatics have already formed rings the transition making them the most likely to soot. The bonding in the alkynes, alkenes, and alkanes cause the difference in sooting for the nonaromatic fuels. Alkynes are the most likely to form acetylene because of its triple bond. The formation of Acetylene is the fuel intermediate leading to the precursors of soot formation [12]. Early data on the critical sooting equivalence ratio for premix flames with air as the oxidizer showed that the sooting tendency decreases in the followed order: Aromatics > Alkanes > Alkenes > Alkynes [12, 36, 40]. Milliken's research showed that the cooler the flame, the greater the sooting tendency for premixed flames. This was later found to be true for diffusion

flames as well [12, 41, 42, 43]. Therefore to properly compare the fuel structure with the sooting tendency, flame temperature needs to be controlled.

In diffusion flames oxygen and fuel meet in the reaction region, which is limited by diffusion. Stoichiometry dictates the temperatures and location of the fuel reaction region. Since stoichiometry is dominating over chemical kinetics in diffusion flame, soot formation is simplified [22]. Soot formation/oxidation times are much greater than the heat release reaction times so consideration only needs to be made for the diffusion times and soot formation/oxidation time [22]. With soot formation/oxidation time being the main factor in determining soot formation then controlling the residence times of the flame becomes a controlling factor in soot production.

1.3 Flame Shapes

The flame shape is an important factor in the recognition of the smoke point. The understanding of the soot formation areas and soot paths can help in the understanding of soot formation. In buoyant flames, soot streamlines converge to the centerline where the fuel is located, as seen in Figure 1.2. When fuel is increased so that a smoke point condition is reached, the flame tip will change from a round tip to a sharp tip. In nonbuoyant flames soot streamlines diverge from the nozzle axis [28]. In microgravity the laminar smoke point condition can occur in two flame configurations: open-tip and closed-tip flames. An open-tipped flame configuration is signified by a blunt tip that occurs because there is no soot present at the flame's axis. The reduction of flow velocities and increase of radiative heat losses with increasing distance from the flame

base provide condition for quenching, and the opening of the tip. A closed-tipped flame configuration occurs when radiative quenching is reduced at shorter residence times [18]. Open-tip flames were observed at large characteristic flame residence times with the onset of soot emissions associated with radiative quenching near the flame tip. Closed-tip flames have soot emissions along the flame axis and open-tip flames have soot emissions form an annular ring about the flame axis [28, 30]. Figure 1.2 shows the soot paths as well as the soot formation results. Soot formation in diffusion flames is limited to fuel-equivalence ratios (φ) of 1-2 shown in Figure 1.2 [30]. For buoyant flames soot is formed near the outside of the flame where φ=1 and then moves inward to the area of cooler and higher fuel concentration. In nonbuoyant flames soot forms near the core where φ=2 and is drawn out to the flame sheet. As nonbuoyant flames start to transition to a smoke point condition they will develop the characteristic horns on the outer edge of the flame sheet. The horns of a sooting flame can be seen in Figure 1.1.

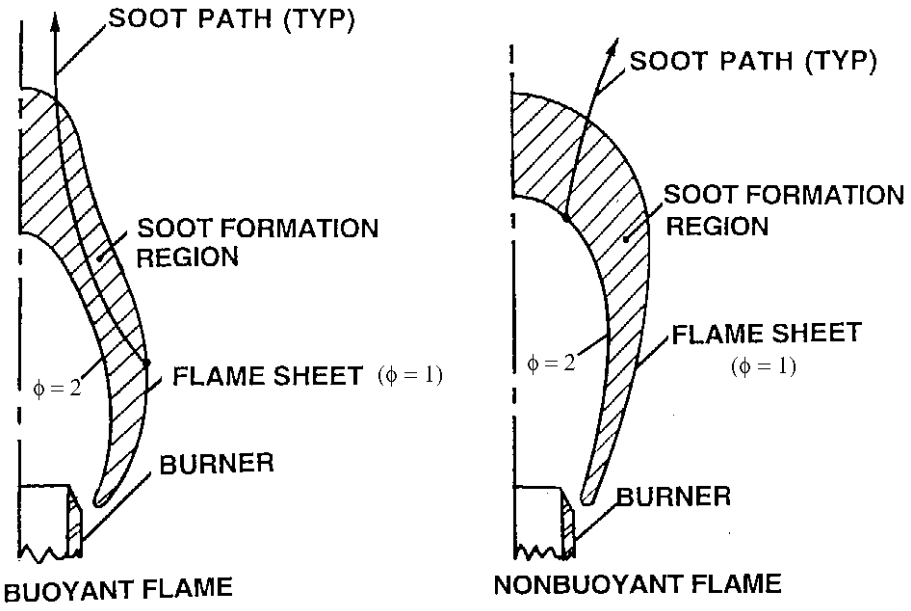

Figure 1.2: Soot path lines through buoyant and nonbuoyant flames

1.4 Buoyancy Effects

Convection is the primary mode of transportation of soot in flames. Soot movement is slightly affected by Brownian motion and temperature gradients [30]. The difference between smoke point properties of nonbuoyant flames and buoyant ones are due to the difference of hydrodynamic properties of the flames [21, 28, 30, 31, 32]. In buoyant flames the flow is accelerating and the streamlines converge toward the axis of the flame. The flow converges to the axis of the flame because of the fuel-rich flame conditions. The difference in nonbuoyant flames is the flow is decelerating and the soot leaves the flame over the extended flame region. The ratio of soot nucleation and growth residence times to soot oxidations residence times are generally larger for buoyant flames than nonbuoyant flames. Residences times are proportional to the square root of flame length in buoyant flames [12, 21, 33]. For the nonbuoyant flames that Dotson observed, residences times are not constant [10]. The soot pathlines can be seen in Figure 1.2.

It is difficult to avoid buoyancy effects on earth even when using parabolic aircrafts and drop facilities. Drop tests have limited test times and parabolic aircrafts have g-jitter affecting microgravity smoke points for four different types of fuels in the International Space Station [10]. Before smoke points were found for nonbuoyant jet flames, it was thought that smoke points would not occur [12]. Urban reported that for comparable flame conditions nonbuoyant smoke point lengths were up to 2.3 times shorter than when tested in ground-based microgravity facilities and up to 6.4 times shorter than buoyant smoke point lengths [30].

1.5 Velocity Field Effects Coflow

Laminar smoke point properties are measured from round buoyant jet diffusion flames with coflowing air. The coflowing air is used to prevent the flame pulsations that occur in the buoyant diffusion flames in still environments. Variations in the velocity field change flame shapes and residence times in the soot formation and soot oxidation region. The sources of velocity change in coflowing experiments are through burner diameter variations and coflow velocity variations. Reducing the burner nozzle diameter increases the mean jet fuel velocity and reduces the flame residence time. For nonbuoyant flames Dotson found that smoke points followed $d^{-0.91}u_{air}^{0.41}$ [10]. According to Dotson's correlation, the diameter of the nozzle has a larger effect on the smoke point than coflow velocity in an inverse fashion. This correlation agrees with the work of Kent and Wagner [10, 27] on centerline soot profiles. Reduction in burner diameter caused the soot volume fraction profile to shift downstream. With the shift in soot volume fractions downstream, flame lengths increase from the decreasing soot formation region.

Coflow velocity also plays a role in the smoke point characteristics of the fuel. Faeth found that as coflow velocity was increased, the soot emissions were suppressed. For nonbuoyant flames there is no buoyancy related acceleration which will tend to dominate to flow path of the gasses and soot. Without coflow nonbuoyant flames decelerate and the velocity of the coflowing air can be used to modify the residence time of the flame. Lin and Faeth examined flames at low pressures where buoyancy effects were minimized and found that coflow velocity greater effects on weakly buoyant flames

than buoyancy driven flames [27, 35, 38]. Their results did not result in a relation between coflow velocity and smoke point length. A relationship between mass flow rate and coflow velocity was found and is shown in Figure 1.3.

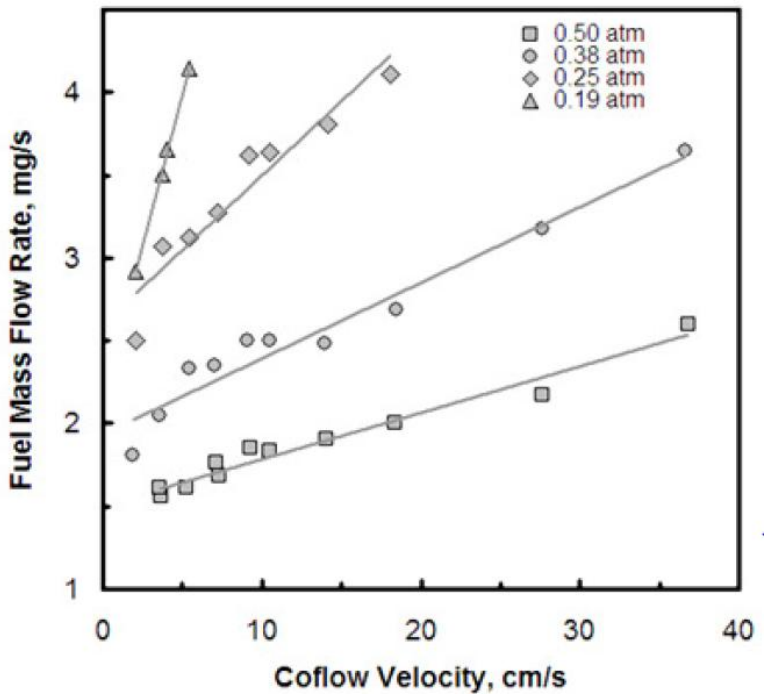

Figure 1.3: The effects of coflow velocity on mass flow rate [35, 38]

The increase in coflow reduced the soot volume fraction which increased the smoke point length. Even in weakly buoyant flames of low pressure flames, the effects of buoyancy driven acceleration changes the effect of coflow velocity. The effects of coflow velocities on buoyant flames are less pronounced than nonbuoyant ones. Schalla and McDonald [36] found that coflow velocity affect the fuel mass flow rate to a point and then leveled off having no effect, as shown in Figure 1.4. This is consistent with the

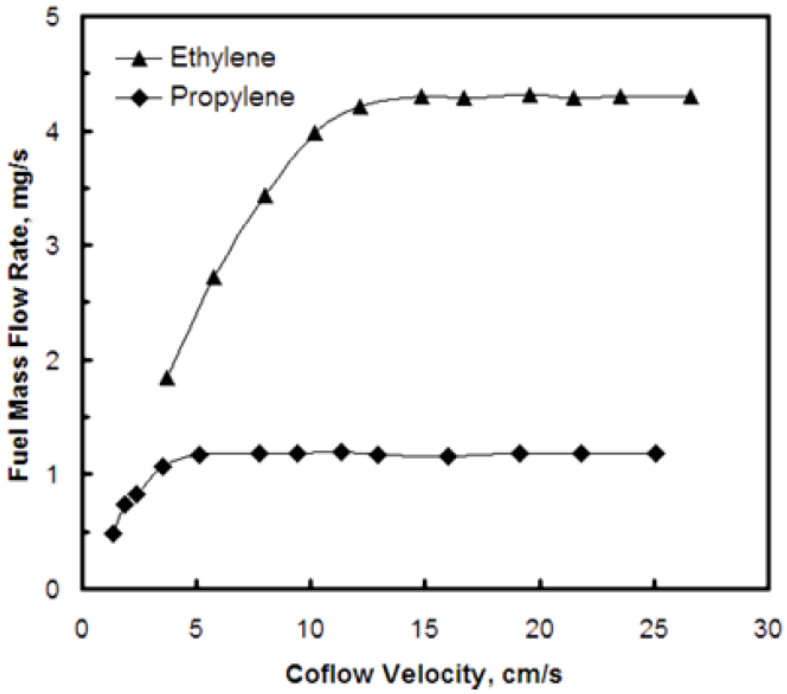

Figure 1.4: The effect of coflow velocity on fuel flow rate [36, 38]

thoughts that buoyant flows dominate the velocity field. A study done by Berry-Yelverton and Roberts [38, 39] showed that ethylene smoke point length increased while the coflow increased. The decrease in the initial fuel to air velocity ratio was associated with an increase in coflow velocity, which increased the smoke point length of ethylene. Schalla and McDonald's test were examined at fuel to air velocity ratios of 0.14 -0.42. Berry-Yelverton and Roberts's tests were done at higher fuel to air velocity ratios of 0.6 - 1.4 and can be seen in Figure 1.5. The effect of coflow velocity is different to buoyant and nonbuoyant flames because of buoyancy driven acceleration. Without buoyancy flames decelerate, as mentioned in the buoyancy discussion, and the effect of the coflow velocity increased.

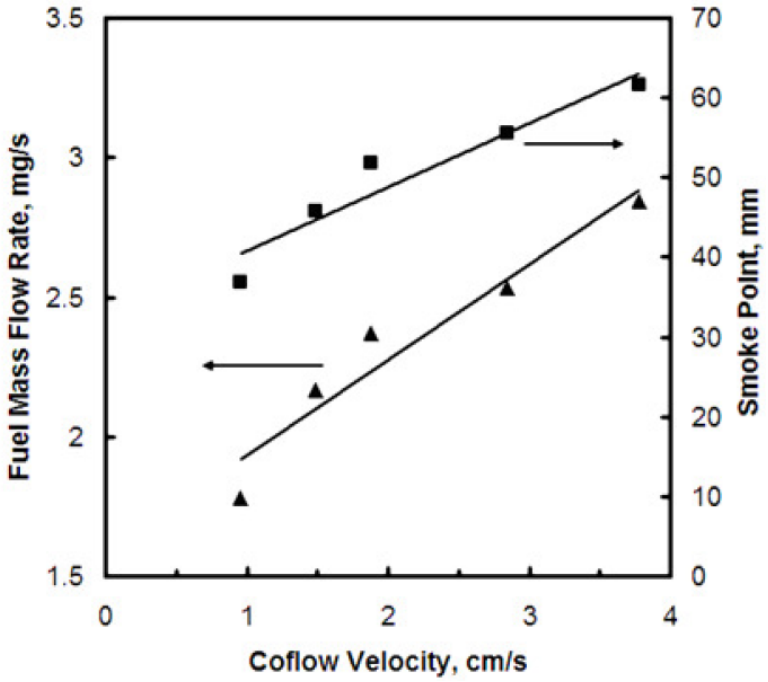

Figure 1.5 Ethylene smoke point length with respect to coflow velocity [38, 39]

1.6 SPICE HISTORY

The first smoke points were reported by Sunderland [21] in a microgravity aircraft. Drop facilities were also used to obtain microgravity, but both had limitations that caused difficulties in the acquisition of smoke point measurements. Urban [18], realizing the time constraints of drop towers and the g-jitter associated with microgravity aircrafts, measured smoke points in Earth's orbit. The measurements were done in quiescent air. Future work focuses on smoke points in coflowing air.

The Smoke Point in Co-flow Experiment (SPICE) goals are to acquire a: better knowledge of and ability to predict heat release, soot production and emissions of fires in microgravity; better design of combustors through improved control of soot formation;

better criteria for flammability of materials for use in next generation spacecrafts. SPICE was developed in 1996 from the Middeck Glovebox and the Enclosed Laminar Flames (ELF) experiment in the Microgravity Glovebox program.

The fires nonbuoyant smoke points were found in orbit aboard the space shuttle Columbia. The International Space Station (ISS) Microgravity Science Glovebox (MSG) began SPICE operations onboard the ISS the in 2009. The result of the operation was 55 smoke points for ethylene, propane, propylene, and propylene/nitrogen mixtures. Tests were done for burner nozzle diameters of 0.41, 0.76, and 1.6 mm and coflow velocities between 5.4 and 65 cm/s. These smoke points led to the lengths scaled with $d^{-0.91}u_{air}{}^{0.41}$, where d is the burner nozzle diameter and u_{air} is the coflow velocity. The scale is also multiplied with a fuel factor A_f, which is a characteristic of the fuel. The SPICE experiment found a difference between the order of soot propensity for fuels when comparing microgravity and normal gravity. The fuel mixtures in microgravity sooting propensity was found to increase as follows: ethylene < propane < 50% propylene < 75% propylene < propylene. The original spice results found by Dotson can be seen in Figure 1.6. A residence time analysis of the flames was done in the original study. The residence times are useful in understanding smoke points, but the analysis did not provide any quantitative correlations [10]. The results from the residence time analysis can be seen in Figure 1.7. Further work on residence time analysis can be seen in K.T. Dotson's 2011 Fire Safety Journal [10].

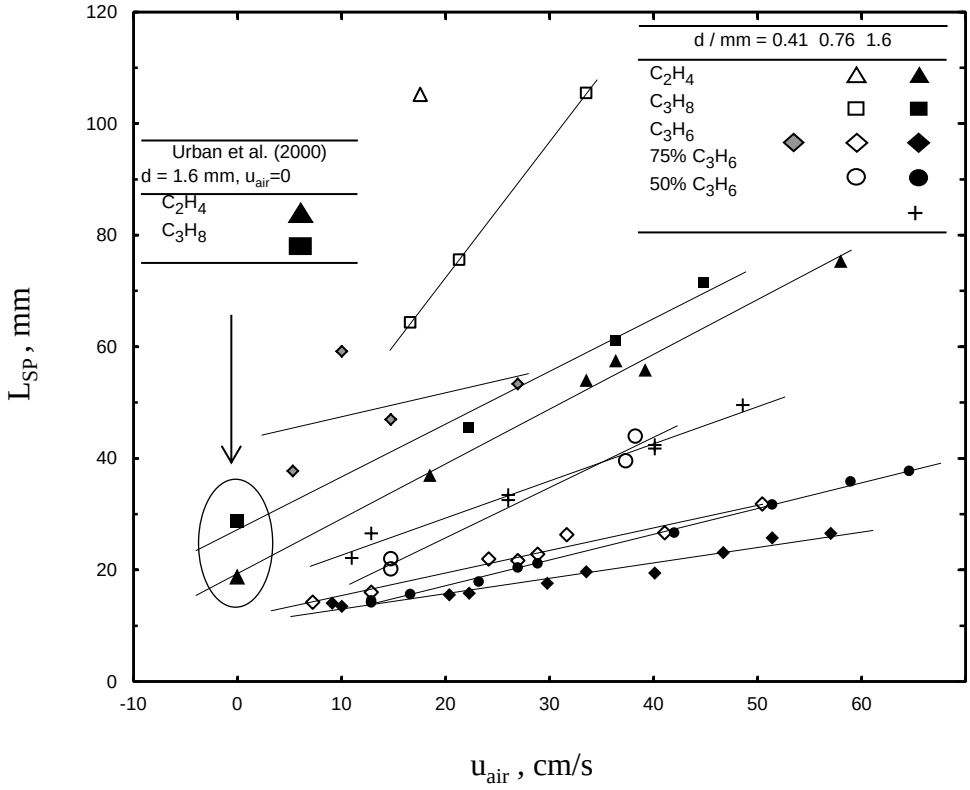

Figure 1.6: SPICE original results adapted from Dotson

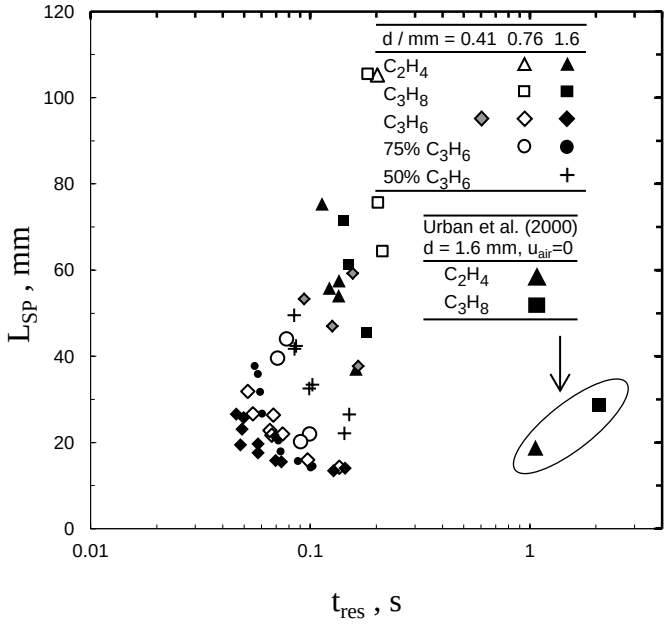

Figure 1.7: SPICE residence time results adapted from Dotson

1.7 Objectives and Contributions

The objective of the SPICE project is to get fundamental data on soot formation. That data can be used in CFD soot models. Smoke point lengths are laminar tests that correlate to soot volume fractions and radiative heat loss fractions in turbulent fires. The smoke point lengths and their use in modeling can help provide an alternative to doing expensive turbulent fire tests.

My contribution to the SPICE project was through video analysis and interpretation of the data that was collected from the tests. The actual tests were done by Don Pettit, a NASA astronaut, and were directed by Dr. David L. Urban. From the videos, 57 new smoke points were found. This data that I collected will be combined with the 2009 flight data throughout the following report. The 2009 data was interpreted by Dotson in his completion of a M.S. in Fire Protection Engineering. Future work done in the SPICE project should reference K.T. Dotson's and my work for comparison of results.

1.8 Computational Fluid Dynamics (CFD)

For CFD models to accurately predict fire growth there are necessary inputs for characterization of the fire. Materials and geometric arrangements affect the burning process. Turbulent buoyant jet flames would be an example of a characterization that is used in CFD models. Delichatsios worked on simple correlations for the relationship between laminar smoke point lengths and smoke yield in turbulent buoyant jet flames

[14]. Laminar smoke point lengths are related to soot volume fractions and radiant fraction of flames. Using laminar data for turbulent flow is useful because of the difficulty and unpredictability of turbulent tests. It is important to have fundamental data set that can be used in these correlations. Since nonbuoyant flames are not driven by buoyant forces, then there is one less parameter affecting the fundamental data. The Fire Dynamics Simulator (FDS) and FireFoam are models that currently use laminar smoke point lengths in correlations for turbulent conditions.

Chapter 2 Test Setup and Experimental Procedure

The Smoke Point In Co-flow Experiment (SPICE) tests were done in order to determine a smoke point length for the various fuels burned. The transitions between smoking and non-smoking flames were sometimes past the video's field of view. The transition between the smoking and non-smoking conditions are indicated by a few key flame shapes. When a flame has transitioned into a smoking flame it changes from a bright luminous rounded boundary at the flame tip to a flame tip with horns. The flame tip opens up and becomes more of a red color because the soot is cooling for release. The test setup and experimental procedure for the SPICE test is important. In order to ensure that the data from the previous flights, the 2012 flight tests being examined, and future flight tests can be compared the experimental procedure and test setup must remain consistent.

2.1 SPICE

The SPICE operations were started in February 2009. The flames were observed in the ISS Microgravity science box. The flames in the 2009 tests were successful and showed a strong impact of the burner diameter and the co-flow air velocity. The strong results called for a reflight and tests were done beginning in February 2012.

The Smoke Point In Co-flow Experiment Reflight (SPICE-R) tests were conducted to expand the knowledge from the first tests. This expansion of knowledge was meant for examining new fuels with a wider range of fuel diameters, as well as

expanding the statistical data that was gained from the first flight. The reflight dealt with pure fuels of Ethane, Ethylene, Methane, and Propane at a range of 0.76-3.2 mm inside burner diameters. The emphasis was to look at pure fuels where the 2009 flights considered diluted fuels as well. The original SPICE burners had inside diameters of 0.41, 0.76, and 1.6 mm where the SPICE-R had 0.76, 1.6, 2.1, and 3.2 mm burners. The SPICE test flight plans included the 0.4 mm burner, but there were no tests done with the burner. The reflight tests were done by astronaut Don Pettit.

The rationale for the reflight was that the previous results have shown a strong relationship with burner size and coflow velocity to microgravity smoke point lengths. Normal gravity smoke points do not show such a strong relationship. Originally there were only three burners tested, the largest being 1.6 mm. The increase in burner sizes to 2.1 and 3.2 mm burners would yield a larger number of smoke points with more fuels. In the previous flight the effect of the burner diameter and coflow velocity was less known. The knowledge gained from the previous flight helped with the creation of the test matrix of the current study to maximize the number of smoke points that could be found.

2.2 Microgravity Science Glovebox

The redesign of the Middeck Glovebox, used in the Enclosed Laminar Flames (ELF) experiment, led to the ISS Microgravity Science Glovebox. The glovebox, shown in Figure 2.1, encapsulates the SPICE module where the flames are examined. The SPICE experimental assembly, shown in Figure 2.2, is a rectangular duct that is approximately

200 mm in length with a square cross section of 76 x 76 mm. The duct has a basic setup from left to right of fan with a ceramic flow straightener, an anemometer for the

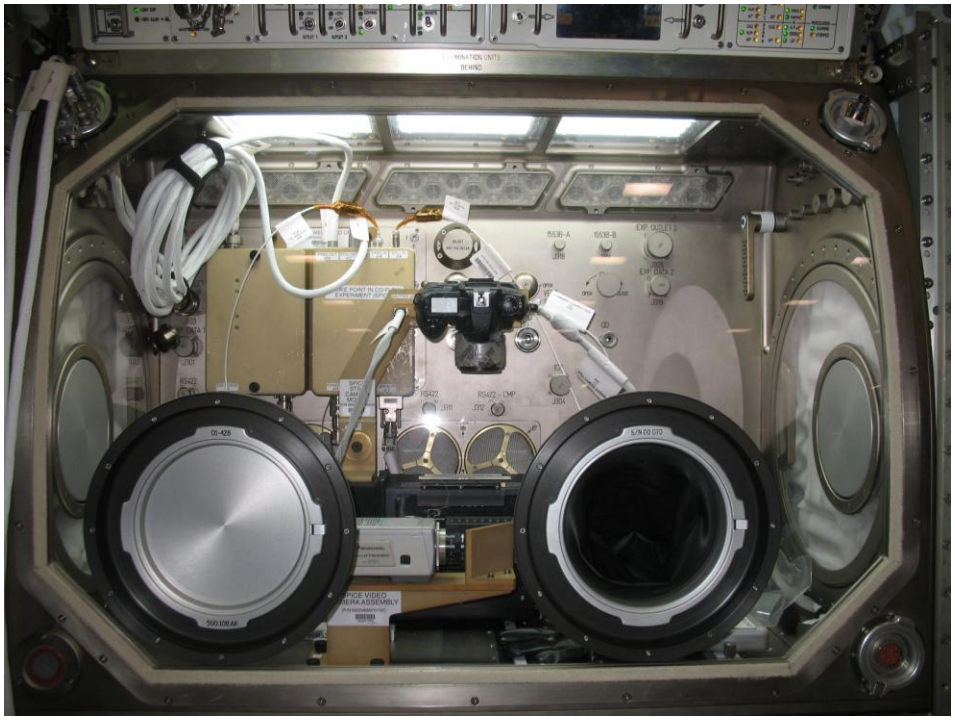

Figure 2.1: ISS Microgravity Science Glovebox

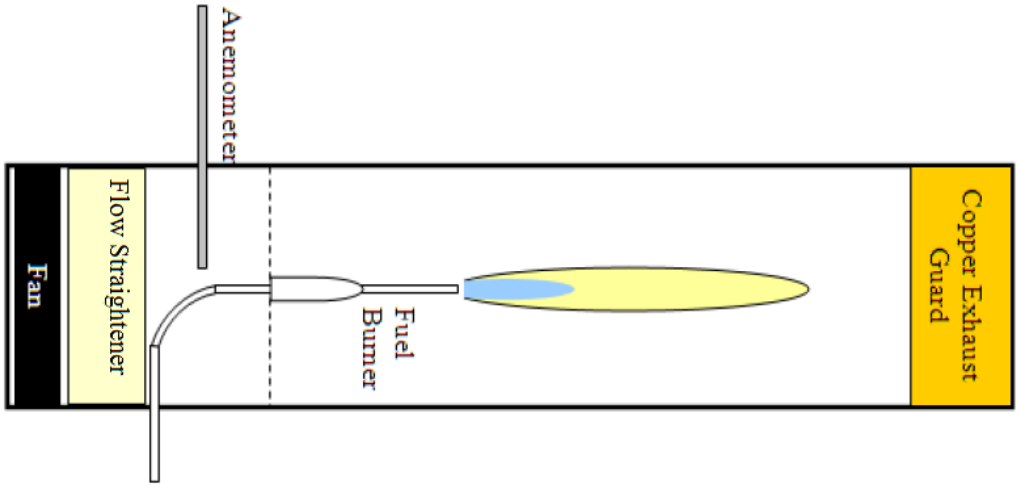

Figure 2.2: Diagram of SPICE experimental chamber adapted from Dotson

air stream, the fuel burner nozzle, an ignitor, an area for flames, and a soot trap for the exit flow. The module's coflowing air is supplied by a DC fan that is connected to a ceramic flow straightener. The ceramic flow straightener reduces the swirling flow of the air from the fan and provides steady airflow to the system. The fan flow is changed by adjusting the air knob on the controller box. An anemometer is used to measure the coflow velocity of the system. Before the air and combustion products exit the flow chamber, they enter a copper screen soot trap to filter the flow. The fuel flow was controlled by the astronaut with the fuel knob on the controller box. 0.76, 1.6, 2.1, and 3.2 mm burner nozzles were exchanged between test runs for the desired fuel diameter. The SPICE experimental assembly is harnessed in the MSG. The MSG includes other

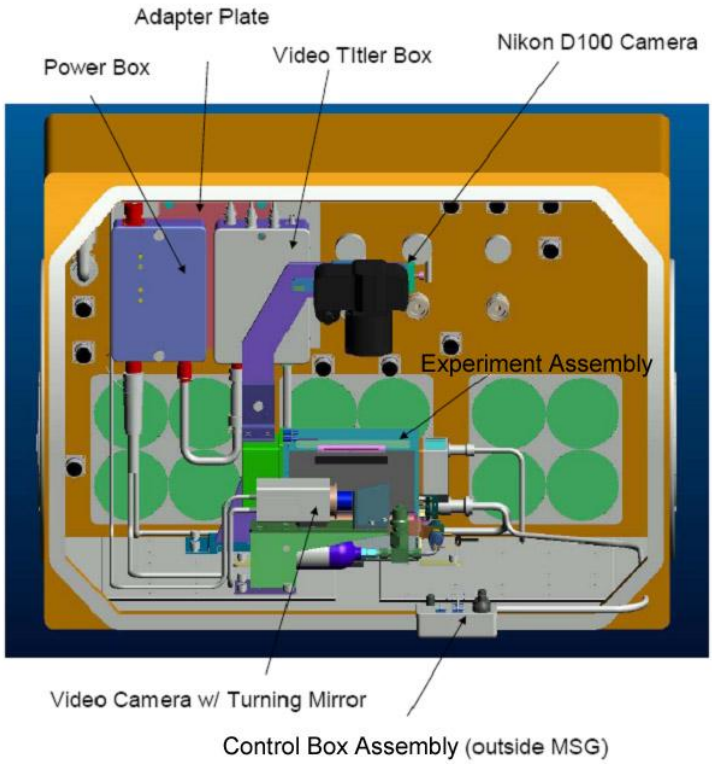

Figure 2.3: The Microgravity Science Glovebox with the SPICE experimental assembly installed inside. The MSG includes all necessary equipment for SPICE.

equipment seen in figure 2.3. The MSG includes the SPICE experimental assembly, a Nikon D100 Camera, a video camera, a control box, power box, and a video box. The Nikon camera is there to supplement the video images with high resolution flame images. The high resolution flame images are taken by the astronaut. The control box controls the fan flow and the fuel flow in the experimental assembly.

The tests were first done test point by test point with ignitions before every test. The astronaut would set the fan setting, adjust the fuel to a beginning setting, ignite the flame, and adjust the fuel flow rate. The fuel flow rate would be adjusted until a smoke point condition was reached. As the experiment progressed the astronaut became more comfortable with the test procedure. Eventually multiple smoke points were found per ignition without extinction of the flame. This procedure change was done in order to save fuel for all of the test points. The ground support crew in Cleveland, OH was guiding the astronaut through the tests indicating when to take pictures and when the flame was smoking. The astronaut was eventually asked to indicate when the smoke point condition occurred because he had the best view of the flame. The astronaut indicated a smoke point conditions with an “elbow wiggle” for the second half of the tests. Propane and a portion of ethane’s smoke point conditions were indicated by the ground crew. The rest of the ethane, the methane, and the ethylene tests were all indicated by the astronaut. A few test runs were done before the MSG was purged and cleaned of the soot. The video was recorded on digital tapes. The videos were then matched up to the audio and compressed into a multi-view video. The compressed videos contained both the video of the MSG chamber and the video of the astronaut.

Once all of the tests were completed and the videos were compiled, the video and camera images had to be analyzed for smoke point conditions. The smoke point conditions were associated with the coflow rates from the video. The camera images, although having much better quality, were not always at the smoke point condition. Smoke point conditions were indicated by the scientists as well as identified through characteristic qualities of a smoking flame. When the smoke point conditions were all found their length were measured in *Spotlight 16*. *Spotlight-16*, a NASA created software package, was designed to perform image analysis for images created by microgravity combustion and fluid experiments. The flame endpoints were indicated by the intensity. The endpoint of the flame was indicated by the intensity reaching fifty percent of the bright yellow body of the flame. Further discussion of flame length measurement can be found in the videography section 2.5.

2.3 Air Meter

The SPICE flow duct anemometer measures the coflow velocity of the system. The anemometer is located on the fan side of the glove box near the fuel burner shown in Figure 2.2. The coflow flows through the SPICE experimental assembly shown in Figure 2.5. The preflight fan calibration was done by Denis Stocker with the results shown below in Figure 2.4. "AIR" reading is correlated to $y = -0.0044x^2 + 1.2899x - 11.828$ in cm/s as shown in Figure 2.4. The fan provided co-flow velocities ranging from 5 to 50 cm/s. A knob that controls the coflow velocity adjusts the fan flow and changes "AIR" and "FAN" readings on the MSG video display. It is important to note that the

fan calibrations were done in normal gravity and the readings show some minor day-to-day variation.

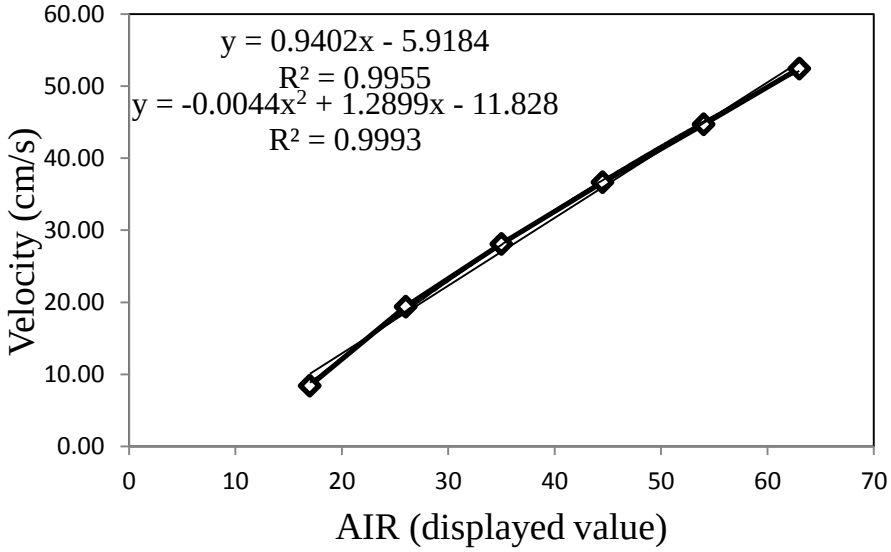

Figure 2.4: The velocity as a function of AIR value. Calibrations done by Dennis Stocker, 2/3/2012.

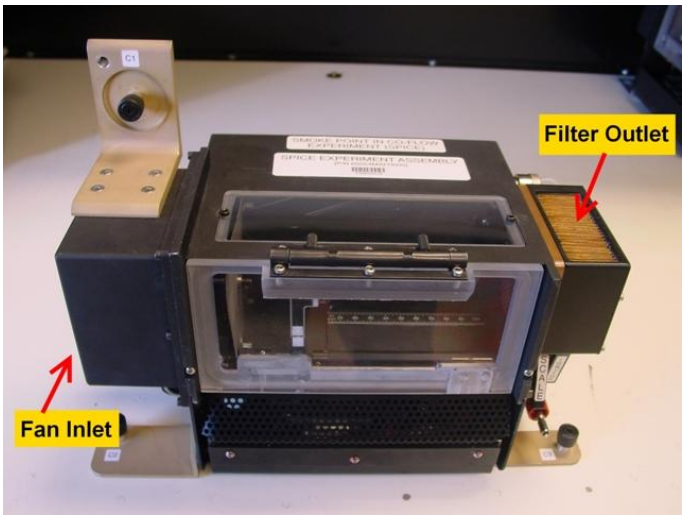

Figure 2.5: SPICE Experiment Assembly. NASA Fan Inlet/ FilterOutlet.

2.4 Fuel Meter

Sierra® manufactured the mass flow controller used for the variation of the fuel flow in the SPICE experiments. The mass flow controller provided the required fuel range of 25 to 500 standard cubic centimeters per minute (sccm). The controller gives the volumetric flow as if the fluid was nitrogen at 21°C and 101.325 kPa. A gas constant K is needed to convert the flow from terms of nitrogen to terms of the specific gas in question. The equations are as follows:

$$Q_{fuel} = KQ_{N2} \qquad K = \frac{1}{\sum_i {X_i}/{K_i}}$$

where K is the is constant for the gas and X is the mole fraction of the gas. K can be calculated for mixtures of gases, but in the extension of the SPICE study only pure gasses were used. Table 2.1 has the relevant K factors for SPICE. The K factor converts the FUEL meter reading to an

Gas	C_2H_6	C_2H_4	CH_4	C_3H_8	C_3H_6-N_2	$3C_3H_6$-N_2	N_2
K	0.5	0.60	0.72	0.36	0.481	0.582	1.00

Table 2.1: K-factor for the gases used in the SPICE experiments. K-factors provided by the manufacturer Sierra.

equivalent volumetric flow rate for the given in sccm. Once the volumetric flow rate was found for the given fuel, a mass flow rate could be derived. The mass flow rate was found through the given conditions and ideal gas law. The conversion is as follows:

$$\dot{m} = \frac{101.325\ kPa * \dot{V}(sccm) * MW}{300.16\ K * 8.314 \frac{kJ}{kgK} * 60 min}$$

The molecular weight and volumetric flow rate of the fuel are the two factors needed for the mass flow rate. The mass flow rates for the corresponding FUEL reading are given in Figure 2.6. It is important to note that while the mass flow rates are relatively similar the fuel velocity can be substantially different between fuels.

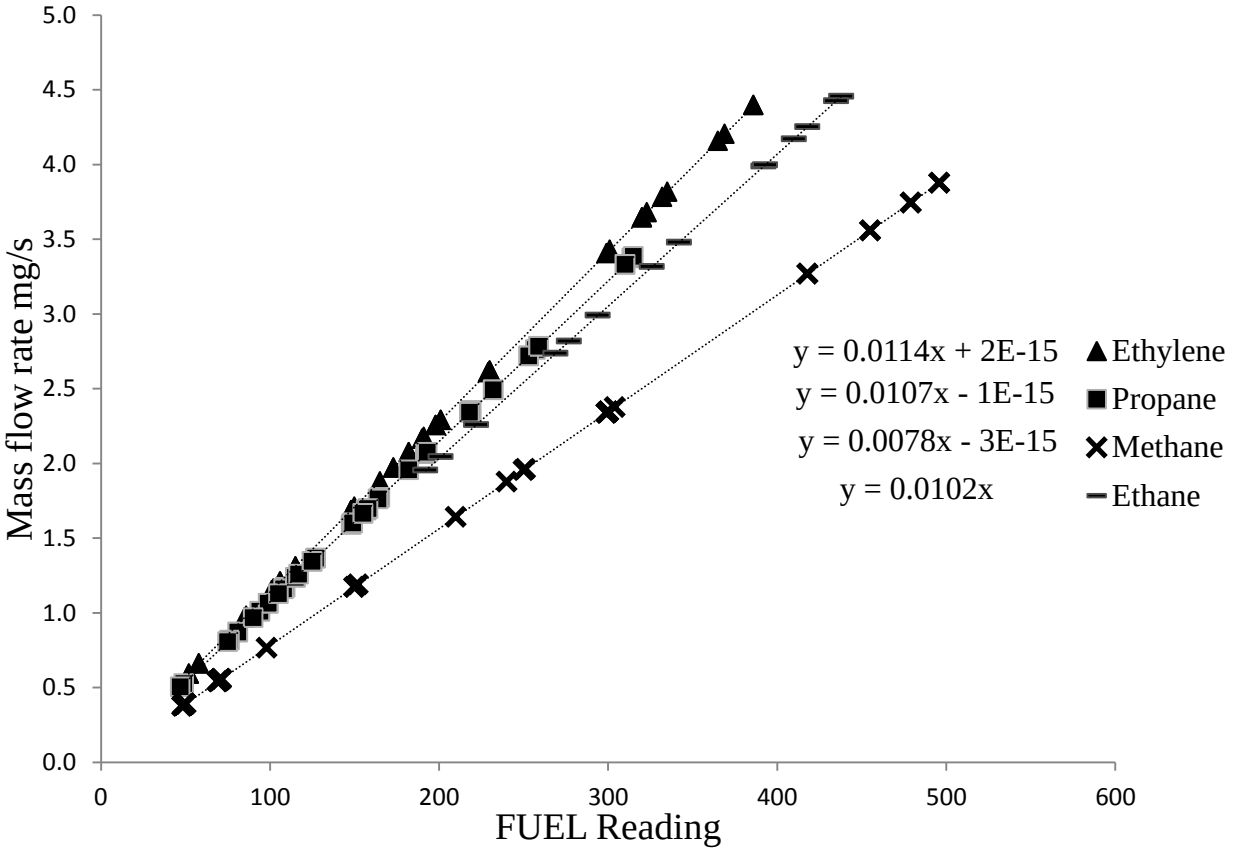

Figure 2.6: Calibrations for the fuel rotameter. Mass flow given in mg/s of the specific fuel.

2.5 Videography

The image analysis was done in *Spotlight-16*, a NASA created software package designed to perform image analysis for images created by microgravity combustion and fluid experiments. *Spotlight-16* is capable of performing analysis on single images or sequences of images. *Spotlight* works with one or more subsets of the image that are called an "Area Of Interest" (AOI). The main function used to find the smoke point length was "Line Profile AOI." The line profile has the ability to count the number of pixels along that line and displays a graph of the intensities along the line. Besides showing the intensity, the AOI can show the minimum, maximum, and mean intensities along the line. The line profile function and luminance plot can be seen in Figure 2.7

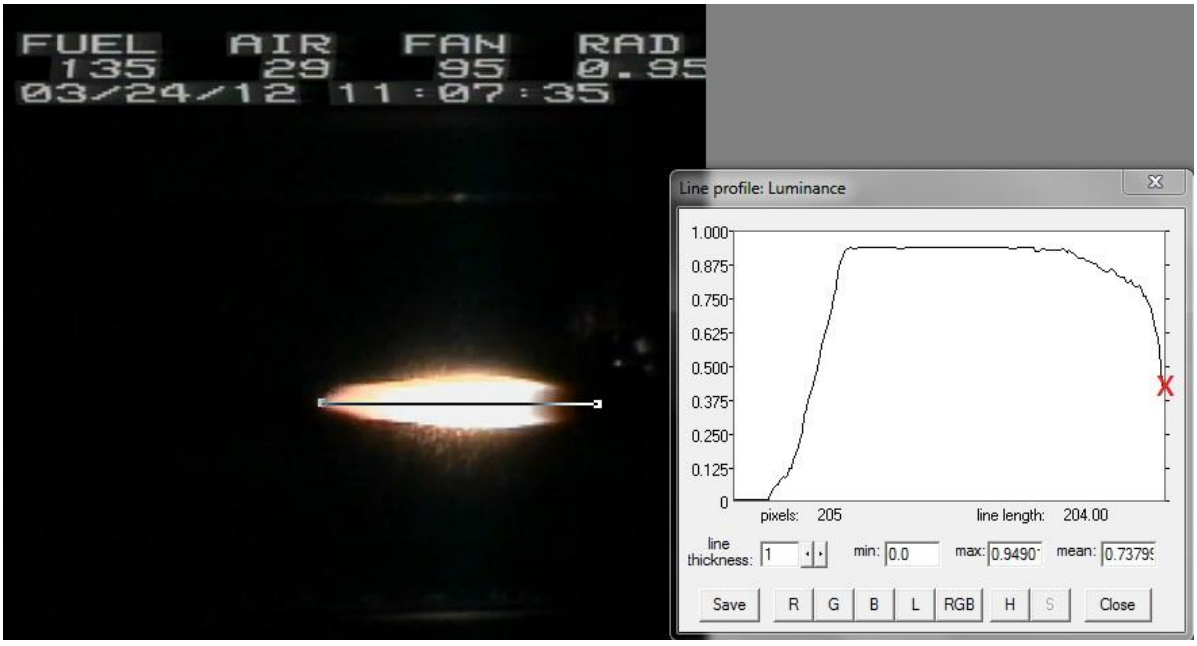

Figure 2.7: *Spotlight-16* Image analysis software. The flame lengths were measured by pixel length. Luminance graph was used to find the end of the flame. The X denotes when the luminosity is at the 50% of the maximum.

The line profile was used to determine the length of the smoke points observed. Before the tests a ruler was shown as a reference to determine the pixel length correlation. After determining the pixel length correlation, flame lengths were found based on the number of pixels. An anchor was set at the end of the burner before each set of tests that denoted the beginning of the flame. The end of the flame length was determined by the intensity graph. When the intensity dipped below fifty percent it was considered to be the end of the flame. An example of the flame length pixel correlation can be seen in Figure 2.7. The pixel length correlation for the uncompressed video was found to be 336.02 pixels per 70 mm. All of the videos were checked for accuracy before measurements were taken.

2.6 Test Procedures

The test procedures for the smoke point flame test were predetermined by NASA. The only part of the testing that differed from run to run was the number of flames that were observed. As the astronaut became more comfortable with the test equipment and procedures, more flames were observed in succession without extinguishment. The succession of tests were performed in order to save fuel. Before each test the astronauts were to refer to their execution notes for the test point number. Then the camera settings were checked and adjusted as needed. The FUEL and FAN flow knobs were rotated to the ignition values given by the test matrix. After the AIR value was verified as greater than five then fuel and ignitor switches, on the SPICE control box assembly, were turned

to “ON”. Once the switches were turned to “ON” then the gas bottle valve must be turned to “OPEN”. Opening the valve released the fuel and the ignitor was immediately pulled forward until the flame appears. After the flame is lit the ignitor should be released. On the SPICE control box assembly the FUEL flow was adjusted to find the smoke point. Initially the procedure involved the ground scientist directing the astronaut to the smoke point. Target points were given to the astronauts as seen in Figure 2.8. Eventually the astronaut was directed to indicate when the smoke point occurred and did

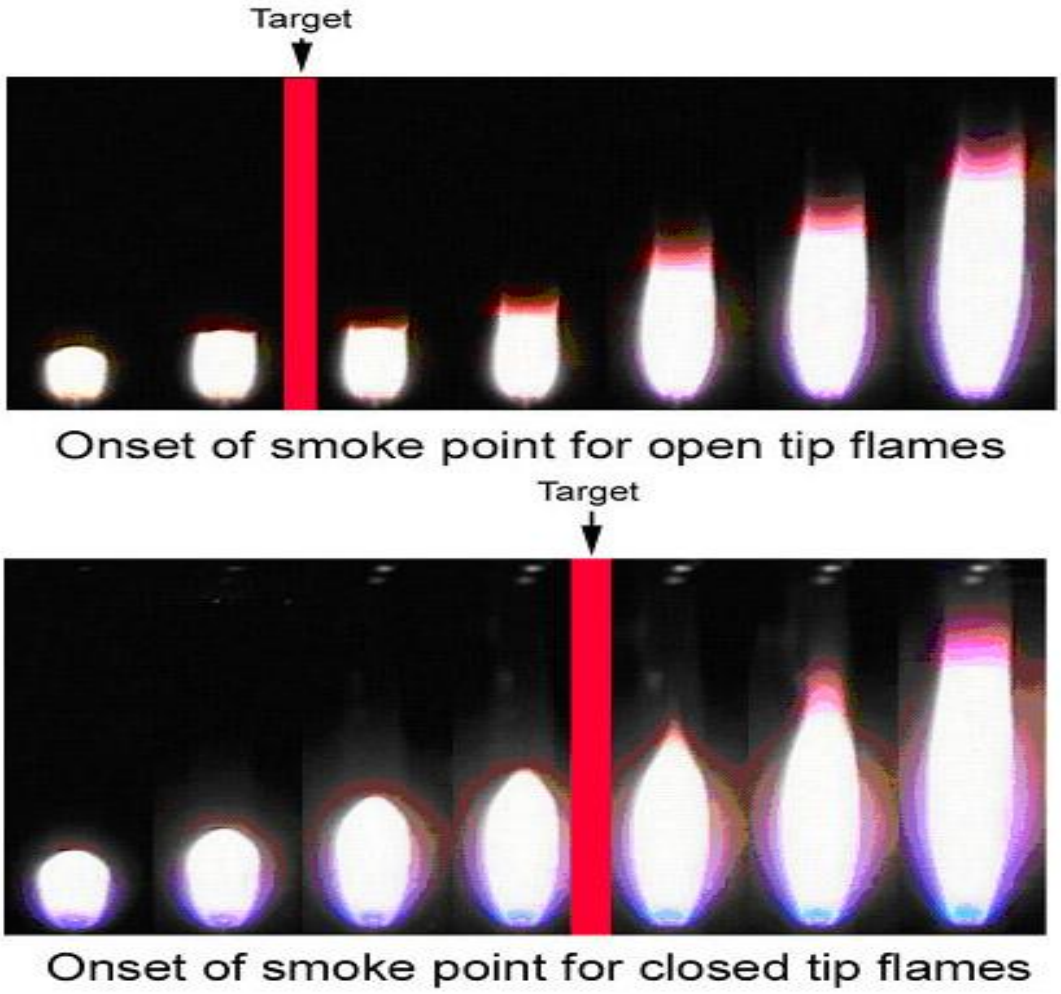

Figure 2.8 Cues for the onset of smoke points for astronauts

so with a shoulder movement. At the smoke point the camera button was pushed, taking a series of images. After the images were taken the FAN was adjusted to the next flow in the run. This was repeated until all the smoke points were found in the run. After the run or set of test points was finished the fuel and ignitor switch were turned off. The test assembly was then setup for the next run.

Chapter 3 Results and Discussion

Smoke points were observed for four different fuels, including two fuels in which smoke points were not previously found. A total of 57 smoke points were found to double the previous study's 55 smoke points to expand to a total of 112 smoke points observed. Smoke point information from this study and Dotson's study can be seen in Appendix 5.1. Smoke points were found for methane and ethane along with more smoke point data for propane and ethylene. In the previous microgravity study done by Dotson smoke points were tested but smoke point conditions were not reached. The flames would reach the copper plate at the end of the duct before approaching a smoke point condition. Some of the fuels that produce less soot smoke points were too long to examine all of the burner nozzle sizes. The smaller nozzles of 0.76 and 1.6 mm were not examined or the tests failed to produce smoke points for methane and ethane. None of the 0.4 mm burner tests were examined for the four fuels because the results would not yield smoke points due to the length. The smoke point information is shown in Table 3.1. Flame images of the smoke points can be seen in the Appendix 5.2. Some of the desired smoke point tests were planned for but not reached due to the limited supply of fuel. There were some additional tests for the 3.2 mm burner of propane. A few of the test points were thrown out due to a smoke point condition not being reached or the smoke point was reached far out of the field of view. Five propane test points were lost due to the flame not being brought to a smoking condition and one ethane smoke point was past the field of view and could not be interpolated.

Fuel	CH_4	C_2H_6	C_2H_4	C_3H_8
d (mm)	3.2-2.1	3.2-1.6	3.2-0.76	3.2-0.76
u_{air} ***(cm/s)***	4.2-15.5	3.0-41.7	3.0-39.1	4.2-39.9
u_{fuel} ***(cm/s)***	66.2-170	19.9-180.3	10.1-714.2	8.4-389.1
Re (fuel)	123.9-211.6	94.7-387.5	36.6-683.1	57.4-788.5
L_{SP} ***(mm)***	75-97.5	44.2-112.1	20.8-115.2	26.5-97.7
A_f ***(mm)***	98.2	64.9	34.8	32.9
Number of Smoke Points	6	13	19	19
Total number of Smoke Points	6	13	25	25

Table 3.1 Results from the microgravity smoke points.

The transition of flames to their smoke points can be seen in Figure 3.1. Figure 3.1 shows the transition from the non-soot emitting flame to the soot emitting flames for the four fuels. The smoke point for each sequence of flames is between the third and fourth flame pictures. Figure 3.1 shows increasing fuel flow at a constant coflow velocity with the increase in flame length for all of the fuels. The four fuels shows the dependence of smoke point length on the type of fuel. Ethane and Methane have much longer smoke points than the ethylene and propane at equivalent coflow velocities.

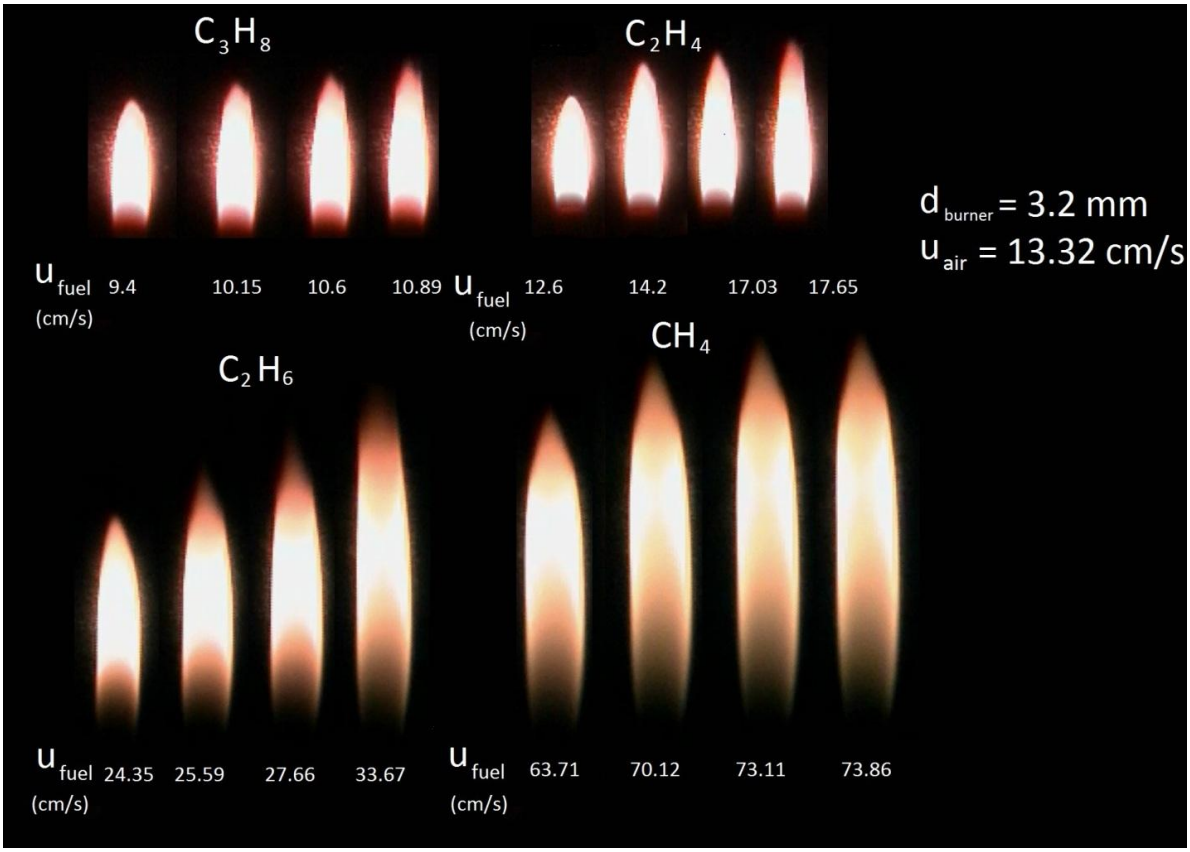

Figure 3.1: Flames at constant coflow and burner diameter with varying fuel flow rates

3.1 Coflow effects

The smoke point lengths are plotted against coflow velocity in Figure 3.2. Smoke point data from the Dotson tests was added to the plot as well, representing all of the microgravity smoke point data found in the SPICE. The linear fits indicate the smoke point data for the given fuel and a given burner size with increasing coflow. Not all the linear fits are increasing with coflow velocity at the same rate suggesting that there are other contributing factors. The smaller burners and cleaner burning fuel increase more

rapidly with coflow velocity. One explanation could be that the increases in coflow velocities decrease the residence time. The decrease in residence time decreases the amount of time in the soot formation region causing less soot production. Another reason for the increase in coflow leading to an increase in smoke point length is through soot oxidation. Increases in coflow velocity could increase the rate of soot oxidation. Coflow contributes less to smoke point length than burner diameter but is still a large contributor and cannot be overlooked.

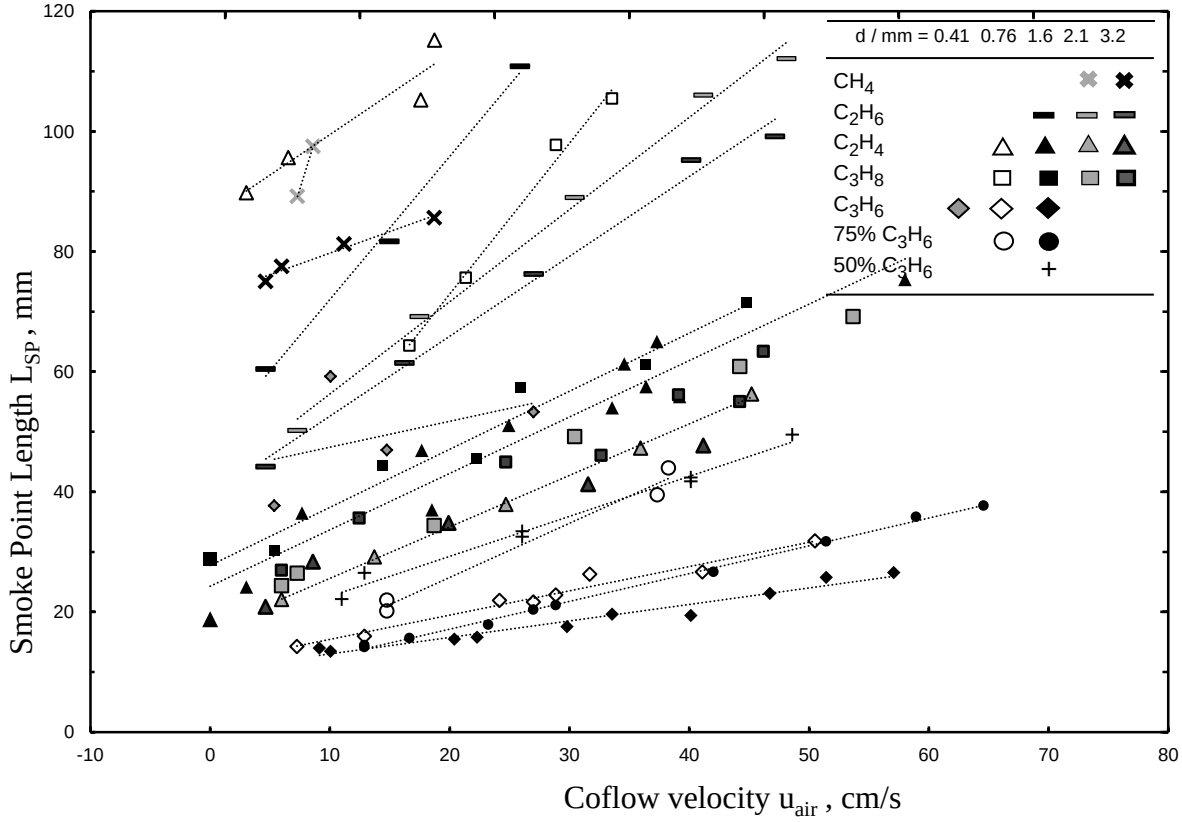

Figure 3.2: Smoke point flame length vs. coflow velocity. The linear fits are shown for each burner diameter for a given fuel.

3.2 Fuel Injection Velocity

Burner size is an important factor when discussing smoke points in microgravity. Burner diameter controls the fuel inlet velocity which by examination of the correlation is dominant over the coflow velocity. Smoke point length increases with decreasing burner diameter. The decrease in diameter creates an increase in fuel jet injection velocity. The increase in injection velocity pushes the centerline soot volume fraction downstream Kent and Wagner's research states [10, 27]. Fuel injection velocity is factored into the residence times of that flame.

Figures 3.3-3.6 show the laminar smoke point lengths at the individual burner diameters. Each plot has a different fuel tested at that individual burner. For the 1.6 mm burner six fuels were tested and given the most data. The plots follow decreasing burner size and increasing fuel injection velocity. Figure 3.3 shows the 3.2 mm burner

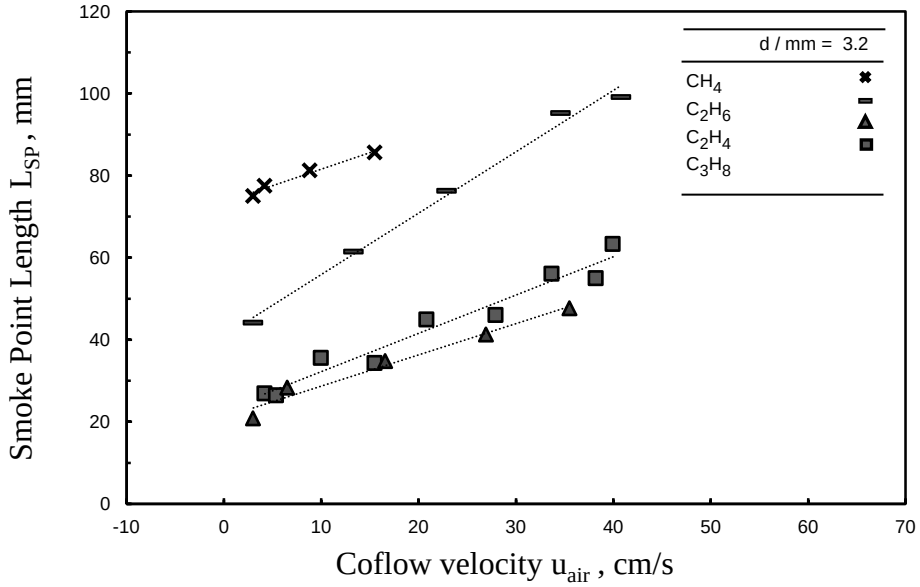

Figure 3.3: Smoke point flame length vs. coflow velocity. 3.2 mm burner only.

having a slight variation in slope from fuel to fuel with the exception of ethane. The similar slopes throughout Figure 3.3 and 3.4 show that the effect of the coflow velocity is very similar at low fuel injection velocities. Switching from fuel to fuel at a larger burner diameter will not dramatically affect the rate of change of smoke point length with coflow velocity. Injection velocities for the two burners range from 8.43 cm/s to 105.4 cm/s with methane being the outlier. The largest injection velocity at these two burners is methane at 153.8 cm/s at the 2.1 mm burner. With only two test points found at the 2.1 mm burner for methane, it is hard to tell whether or not it would fit the same profile as the rest of the fuels. More test points would be needed for methane to add to the analysis of the 2.1 mm burner. Once the tests were switched to the 1.6 and 0.76 mm burners the

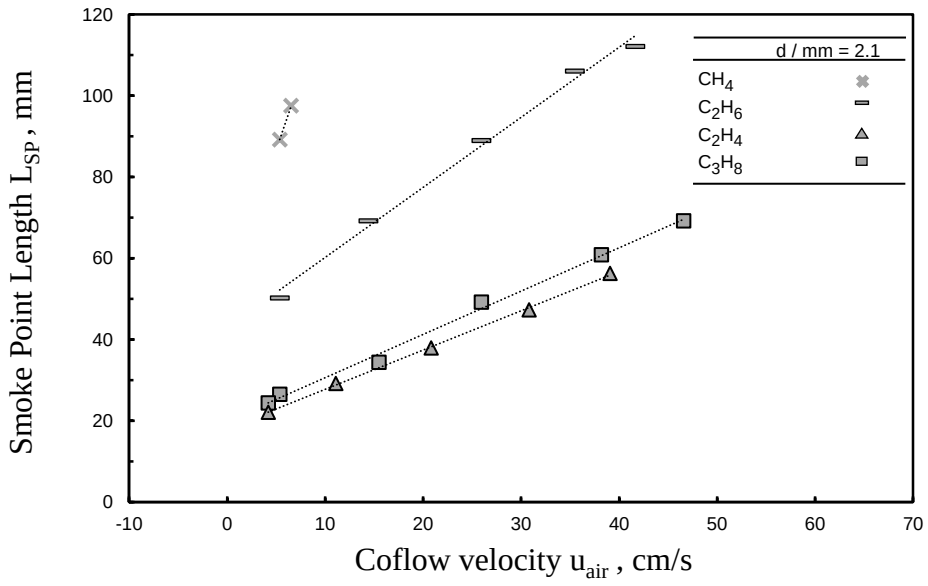

Figure 3.4: Smoke point flame length vs. coflow velocity. 2.1 mm burner only.

results started to produce outliers in changing smoke point length with respect to coflow velocity. Ethane becomes the first fuel to not follow the trend of smoke point length against injection velocity seen in Figure 3.5. It is expected that ethane would not follow

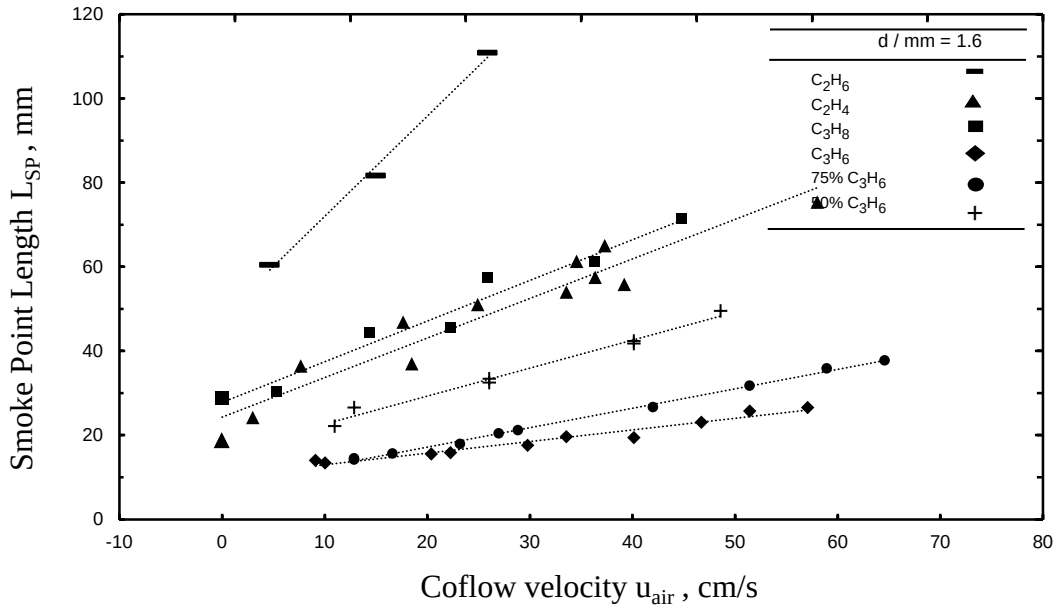

Figure 3.5: Smoke point flame length vs. coflow velocity. 1.6 mm burner only.

the same path with coflow velocity because of its cleaner burning characteristics. Besides ethane all of the fuels increase with coflow at a similar rate. The 0.76 and 0.41 mm burner, seen if Figure 3.6, is when the fuels do not follow the same path with increasing coflow velocity. Ethylene and propane also switch in sooting propensity. At the 0.76 mm burner injection velocities are much higher than previous burners and could be a factor in the change in effect of the coflow velocity on smoke point length.

It is important to notice that there is an increasing change when decreasing the size of the burner. The change in smoke point lengths between the 3.2 to 2.1 mm burners is not as larger as the difference between the 1.6 and 0.76 mm burners. The injection velocity doubles in the first change and is four times as much in the second change. The fuel injection velocity is not linearly dependent with the change in burner size. This nonlinear dependence can account for the degree of increase in the smoke

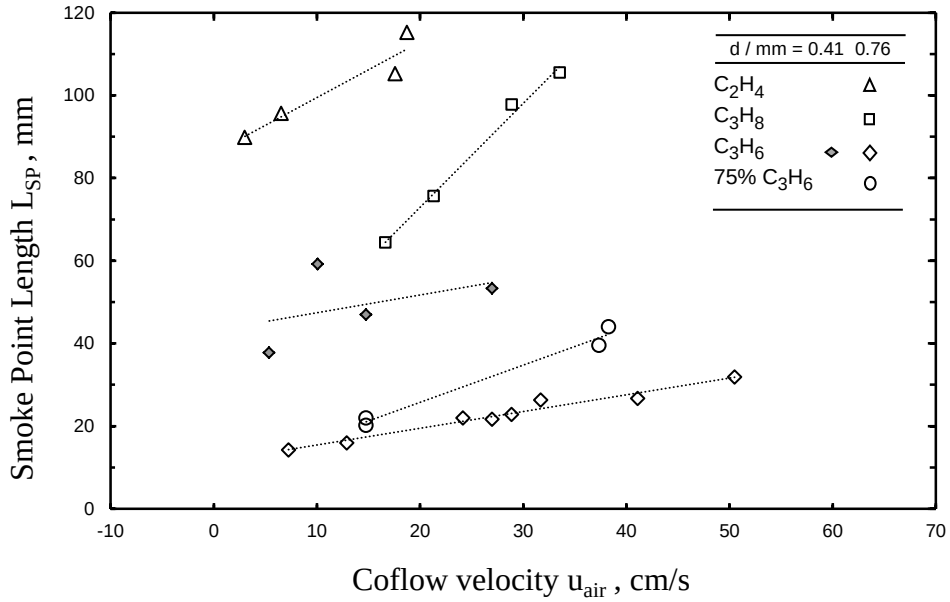

Figure 3.6: Smoke point flame length vs. coflow velocity. 0.76 and 0.41 mm burner only.

point length when examining the 0.76 mm burner. Figure 3.7 shows the difference in injection velocity of the 3.2, 2.1, and 1.6 mm burners against the 0.76 mm burner. The fuels shown are propane and ethylene because they were the fuels that were tested over the full range of burners. The 3.2, 2.1, and 1.6 mm burners for the fuel are all below the 150 cm/s range and are all relatively similar. While the mass flow rates at the same burner size stays close because it is user controlled. The difference between mass flow rates of the fuels is negligible and can be seen in Figure 2.6, the calibrations for the fuel rotameter. The large increase in injection velocity would have less of an effect in buoyant flows. Buoyancy driven acceleration dominates over the injection velocity and the effect of the injection velocity is dampened. When buoyancy is removed from the flow injection velocity seems to become a larger factor in the time the fuel is in the soot formation region.

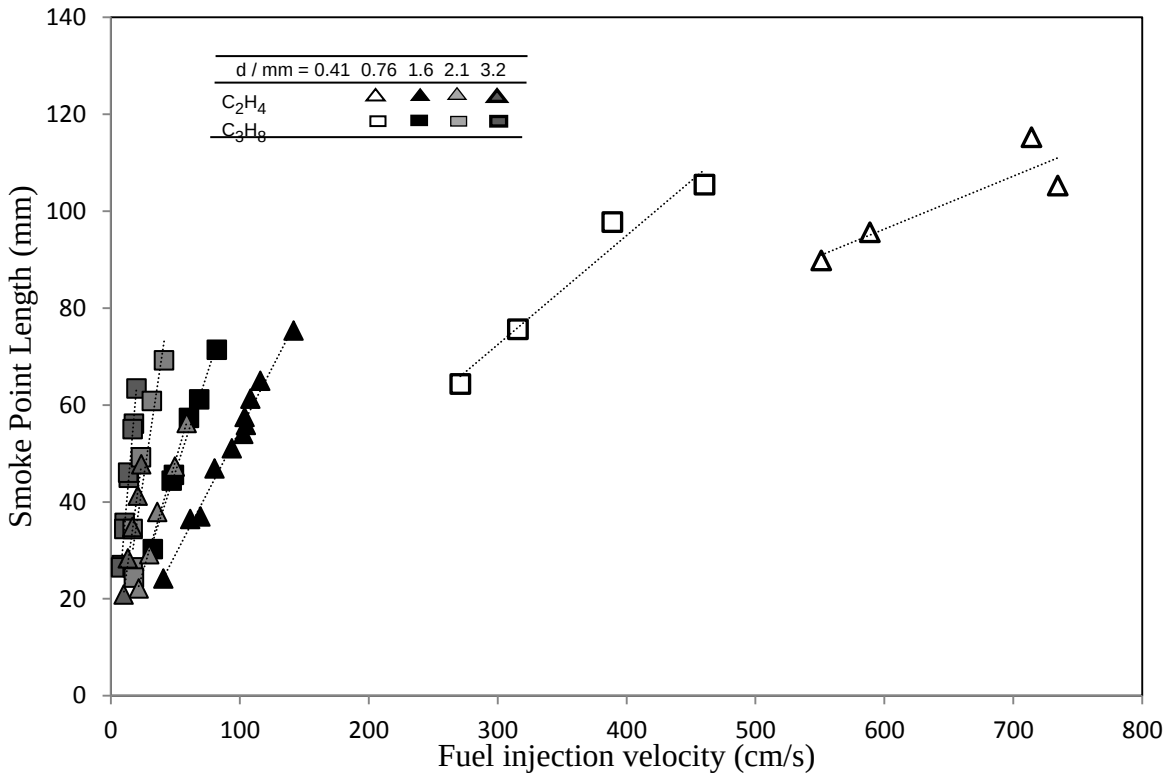

Figure 3.7: Smoke point flame length vs. fuel injection velocity. The linear fits are shown for each burner diameter for a given fuel.

With higher injection velocities at smaller burner diameters it is important to verify that the flow is not turbulent. The Reynolds number for each test is given by:

$$Re = \frac{\rho u_{fuel} d}{\mu}$$

The Reynolds numbers were all under 1000 for the SPICE tests done. The Re < 1000 would suggest that the experiments never transitioned to turbulent flows. Figure 3.8 shows how the smoke point length over diameter changes with Reynolds number of the fuel. The Reynolds of the fuel is driven by the diameter and the fuel injection velocity.

Ethylene at the 0.76 mm burner is an outlier as seen in the other plots. Reynolds data can be seen in Appendix 5.1.

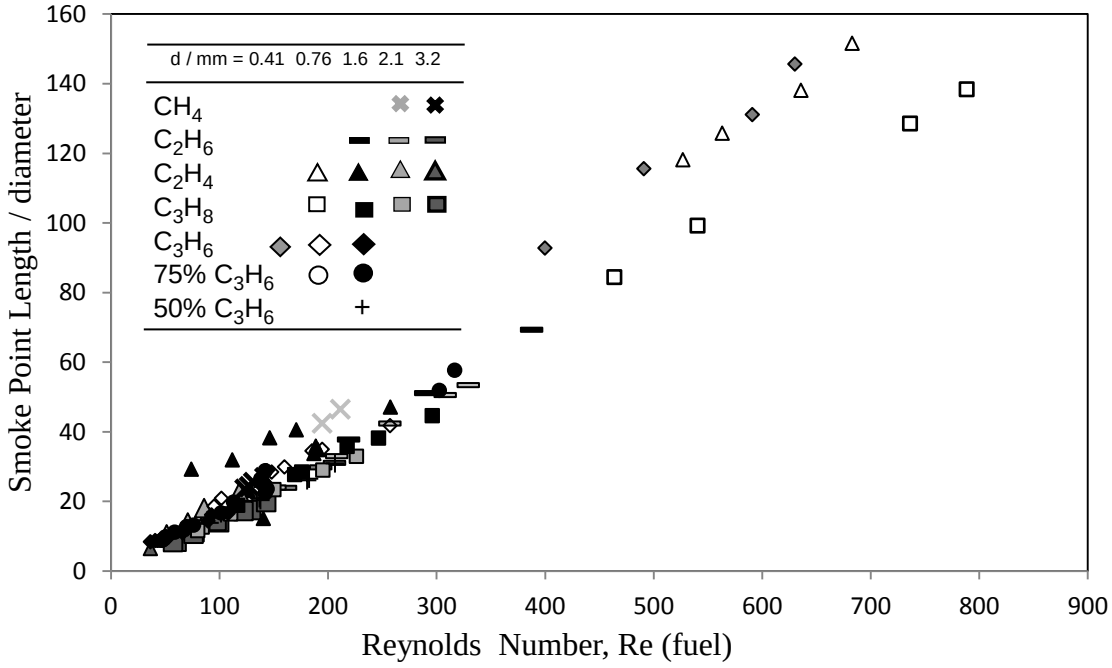

Figure 3.8: Smoke point flame length vs. Reynolds number based on fuel injection velocity.

3.3 Fuel comparison

Methane flames were the longest of the observed smoke point flames with the largest A_f value in the correlation. Tests of only 3.2 and 2.1 mm burners were able to be examined at low coflow velocities. The maximum coflow velocity observed was 15.51 cm/s and can be seen in Figure 3.9. Even with the low coflow velocities the smoke points were larger than the other fuels examined. The methane flames were less luminous than their sooty counterparts. The flames grew in luminosity as they grew

longer. Methane flames throughout the tests were open tipped flames. Their smoke points were identified by the horns associated with smoke points. The horns are less pronounced than other fuels because of the methane's small propensity to create soot.

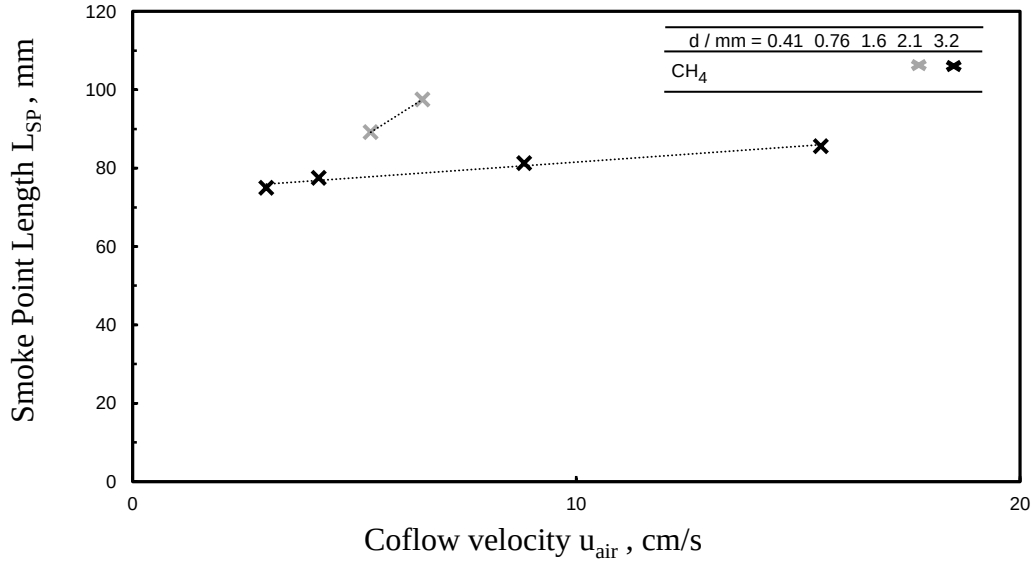

Figure 3.9: Standard pressure nonbuoyant methane smoke point lengths.

Ethane flames had the next longest smoke point lengths. Ethane smoke points were tested for 3.2, 2.1 and 1.6 mm burners. The 1.6 mm burner tests began to pass the edge of the field of view and the tests were stopped. Ethane flames were clean burning, but were more luminous than the methane flames. The ethane smoke point was signified by the transition to an open-tip flame with horns. As the coflow velocities increased the smoke point condition came before the transition to an open-tipped flame. The smoke point occurred when the flame was still closed tip. The smoke point was recognized by the reddening of the flame tip. The decrease in burner size saw the same result. In the 1.6 mm burner, closed tip smoke points occurred at much lower coflow velocities. The ethane smoke point results are shown in Figure 3.10.

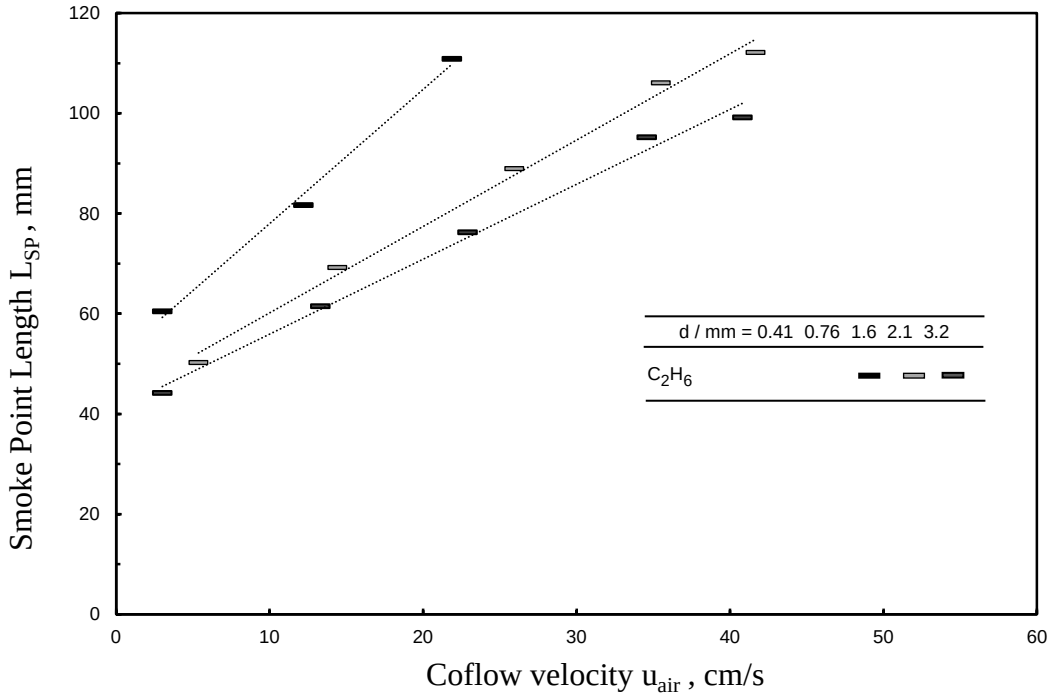

Figure 3.10: Standard pressure nonbuoyant ethane smoke points lengths.

Propane and ethylene had the greatest propensity for soot. Their smoke points were identified by the dimming, reddening, and rounding of the flame tip. The horns seen at a smoke point condition were more visible in the higher sooting propane and ethylene. The propane and ethylene flames have close smoke point lengths until the 0.76 mm burner as seen in Figure 3.11. When the 0.76 mm is reached the smoke point of ethylene greatly lengthens and becomes longer than the propane smoke points. This counters the results from the other burner sizes as well as what happens in normal gravity. For the 3.2, 2.1, and 1.6 mm burners propane flames have longer smoke points than the ethylene flames at respective burner sizes. This relationship is consistent with normal gravity smoke points in coflowing air. The other fuels followed the recognized

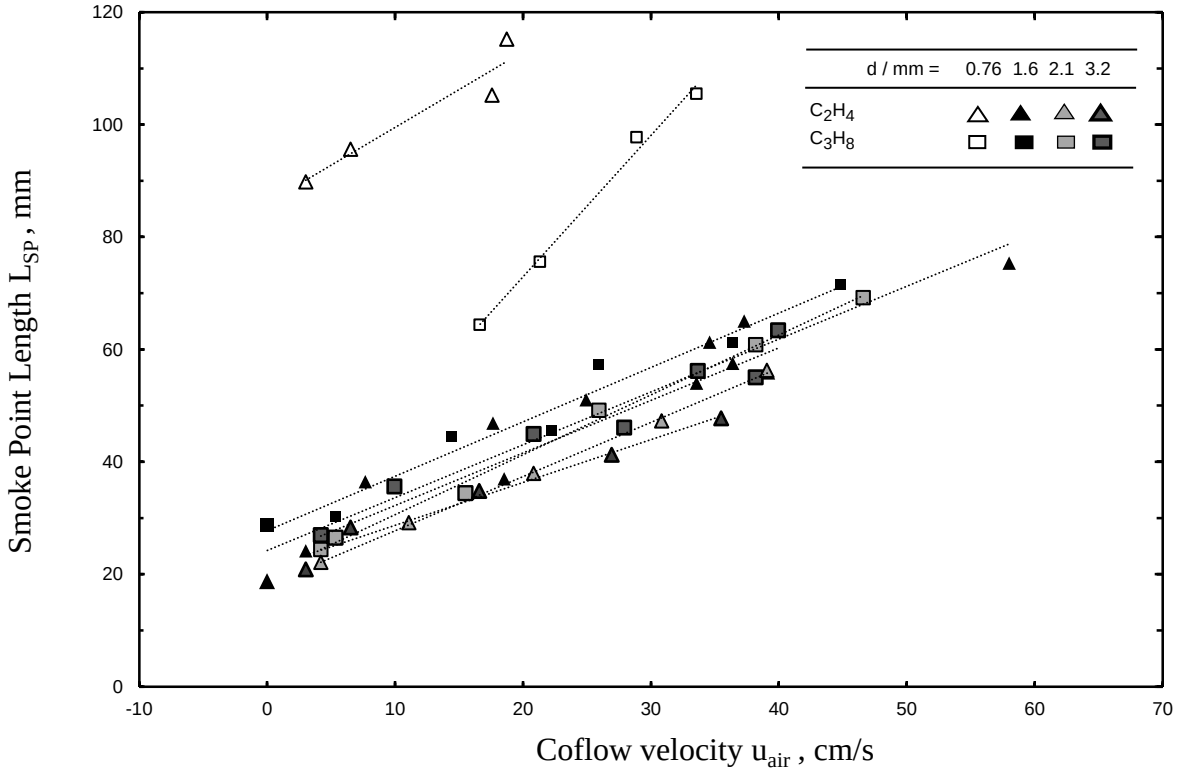

Figure 3.11: Smoke point flame length vs. coflow velocity for ethylene and propane. The linear fits are shown for each fuel. Ethylene and propane smoke lengths are relatively similar except in 0.76 mm burner.

order of smoking diffusion flames: Aromatics > Alkynes > Alkenes > Alkanes. Ethylene does not follow the conventional form for a 0.76 mm burner in nonbuoyant conditions and its mechanisms need to be examined for a better understanding of the result.

The sooting propensity based on the derived A_f values is as follows from least to greatest propensity: methane (98.2) < ethane (64.9) < ethylene (34.8) < propane (32.8) < 50% propylene (20.04) < 75% propylene (12.15) < propylene (10.37). Values for propylene were rederived based on their new fit in the correlation. The order of sooting propensity is contradictory with normal gravity, which is discussed in the following

section. Normal gravity tests yield the results: methane < ethane < propane < ethylene < 50% propylene < 75% propylene < propylene. The A_f values with respect to normalized 1g gravity smoke points can be seen in Figure 3.12. The normalized smoke point lengths were obtained from Li and Sunderland [1]. It is important to note that ethylene has a larger A_f value than propane while having a shorter normalized smoke point length.

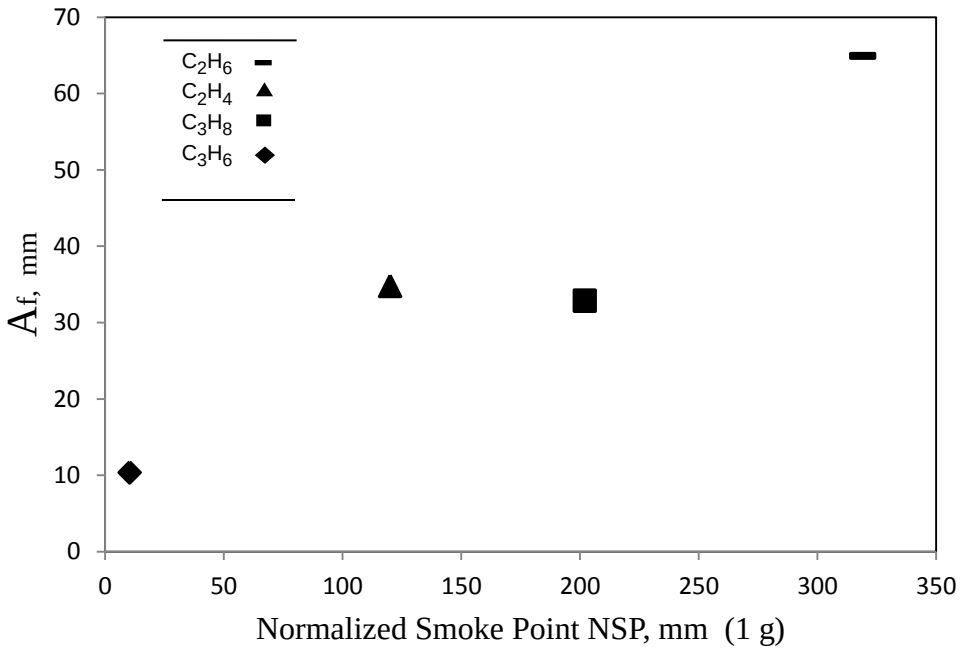

Figure 3.12: The derived fuel factor, A_f with respect to NSP of normal gravity flames from Li and Sunderland [7].

3.4 Correlation

The original correlation of smoke point was of the form $L_{SP} = A_f d^a u_{air}^b$, where d is in mm, a and b are fitted constants, u_{air} is in cm/s, and A_f is a constant derived for each fuel in mm. Data from Dotson's previous study was combined with the current

study to update the correlation. The correlation quantifies smoke point length's dependence of burner diameter, coflow velocity, and fuel. The *a, b,* and A_f values were determined from maximizing the R^2 of the fit while the slope of the fit remained a constant one. Once the exponents a and b were set the fuel A_f was found by maximizing the R^2 value of the correlation. The original study done by Dotson lead to the a= - 0.910 *b*= 0.414 values used for smoke point length estimation. The exponent's respective signs of positive and negative are consistent with the previously discussed effects of coflow and diameter change. As more fuels and data were added and more data was added that correlation was no longer applicable. The original correlation done by Dotson can be seen in Figure 3.13.

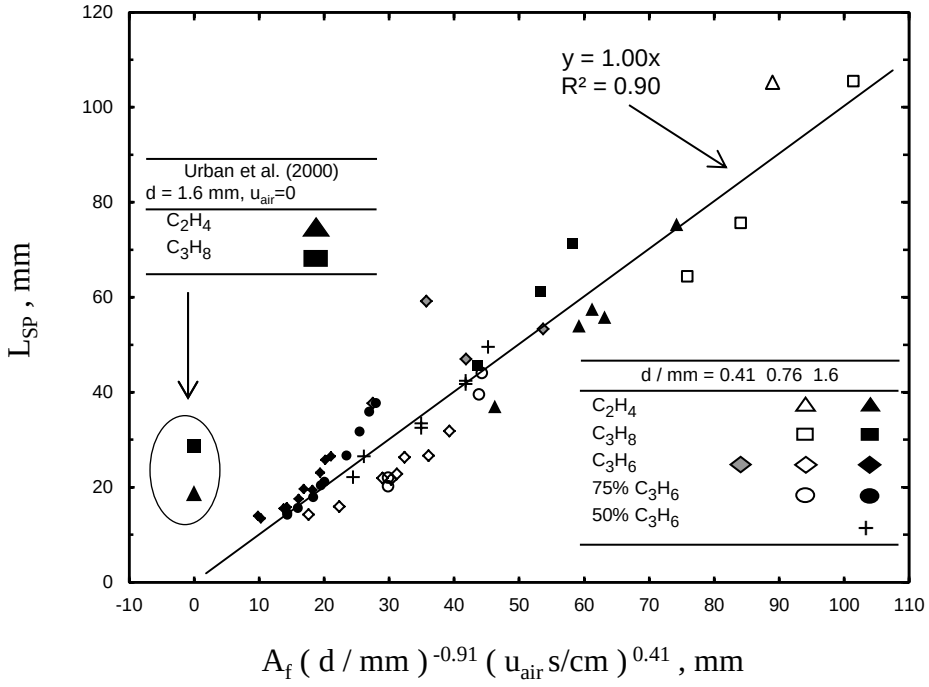

Figure 3.13: Smoke point flame length and scaled correlation. Original correlation found by Dotson.

With two more fuels and more than double the original data the correlation had to be updated to reflect the new data. The addition of the new smoke points brought the original correlation R^2 value to a value close to 0.8. The scaling can be seen in Figure 3.14 and it is important to mention that the data from Urban [18] is not included in the statistical fit. The original format, $L_{SP} = A_f d^a u_{air}^b$, of the scaling was kept because of its connection with the data. However, when the new data was analyzed new *a*, *b*, and A_f

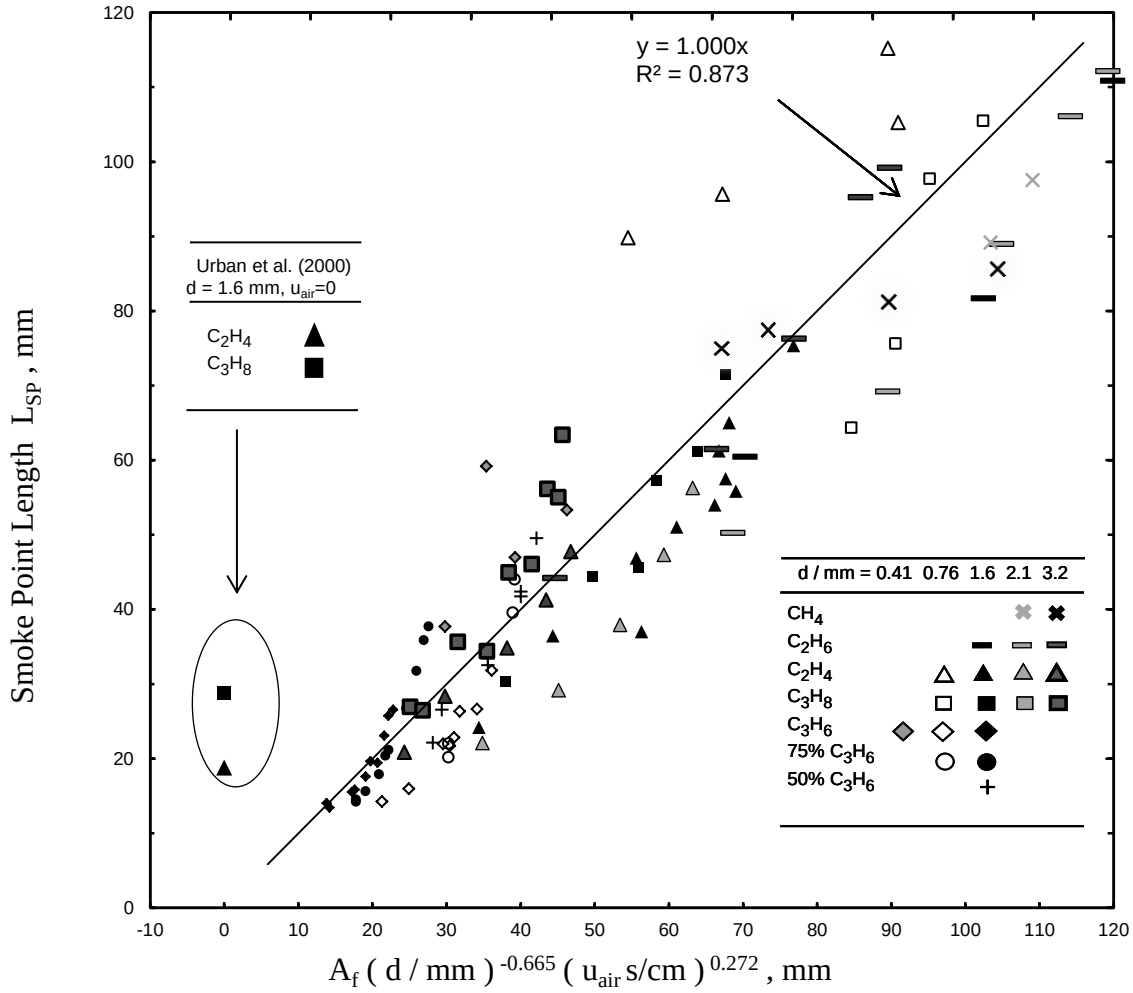

Figure 3.14: Smoke point flame length and scaled correlation. All of the data found from the MSG was used to update the correlation.

values were determined from maximizing the R^2 of the fit. The updated correlation values found in this study are a= 0-.665 and b= 0.272. These updated exponents better reflect the cumulative data set. The updated A_f values can be seen in Table 3.2 along with

Fuel	CH_4	C_2H_6	C_2H_4	C_3H_8	50 % C_3H_8	75 % C_3H_8	C_3H_8
A_f **original**	N/A	N/A	21.2	18.5	13.9	7.65	6.05
A_f ***(mm)***	98.21	64.92	34.8	32.88	20.04	12.15	10.37

Table 3.2 The change in fuel factors from the original study to the current study

the previously derived fuel factors. With the addition of new data, the R^2 of the fit reduce from 0.90 to 0.873 with the addition of the new data. The reduction in the R^2 ofthe fit is to be expected because of the number of data points that were added. Another factor to the reduction of the R^2 value was the addition of more 0.76 mm ethylene smoke points. The smoke points for ethylene at the 0.76 mm burn do not follow the correlation well. The difference between the correlation for the ethylene smoke point length and ethylene's measured smoke point length can be seen in Figure 3.15. Ethylene was the fuel that did not recognize the order of diffusion flames given earlier by Glassman [29]. Without the four Ethylene points in the 0.76 mm, the correlation could be refined to a R^2 value of 0.93 seen in Figure 3.16. The exponents of the correlation would change to a= -0.5 b= 0.34. The effect of coflow increases. This increase is because at the 0.76 mm burner the diameter of the burner starts having a larger effect than previous burner sizes. However, further testing would need to be done to find the dominating factors affecting these test points. In Sunderland's [38] method of normalizing smoke points propane has

the greater smoke point length. The differences in the fuel need to be examined molecularly to give thought to this change. Propane consists of only

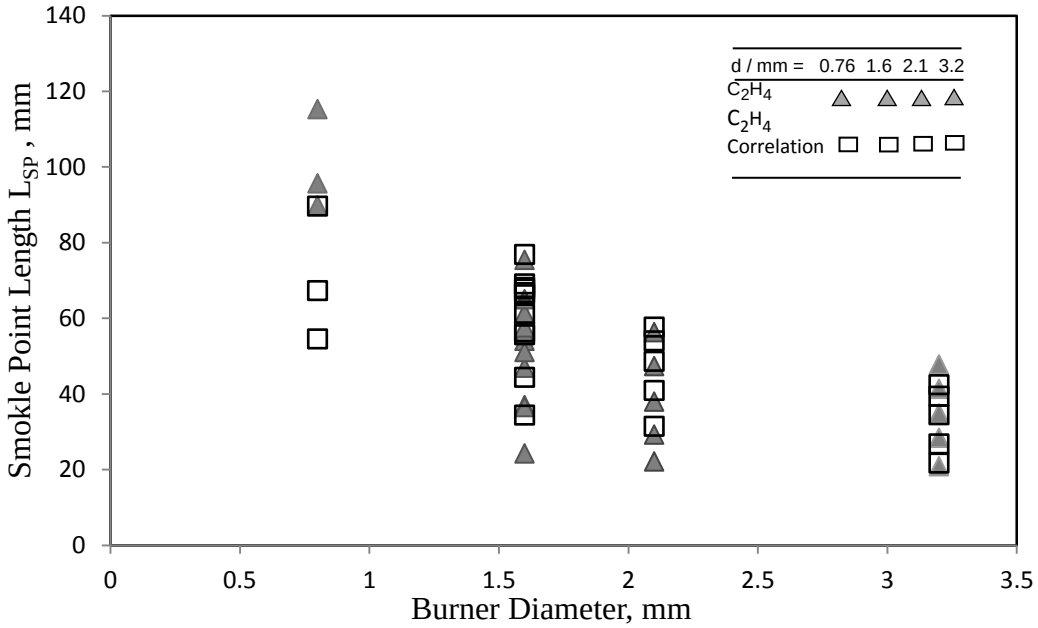

3.15: A comparison of the measured smoke point data to the correlated smoke point data for ethylene.

single bonds which give it a lower propensity to soot than a double bonded ethylene. This would back up the theory and results of propane being a less sooty flame.

There is a difference in molecular weight between C_3H_8 (44.1 g/mol) and in C_2H_4 (28.05 g/mol) that can be explained by the residence time theory of microgravity smoke points. In microgravity there is greater control of residence time. The lower fuel velocity of propane increases the available time for soot formation. With a longer available time for soot formation the propane would have a higher propensity to soot. The jump in fuel velocity from the 1.6 mm burner to the 0.76 mm burner is more pronounced. The fuel

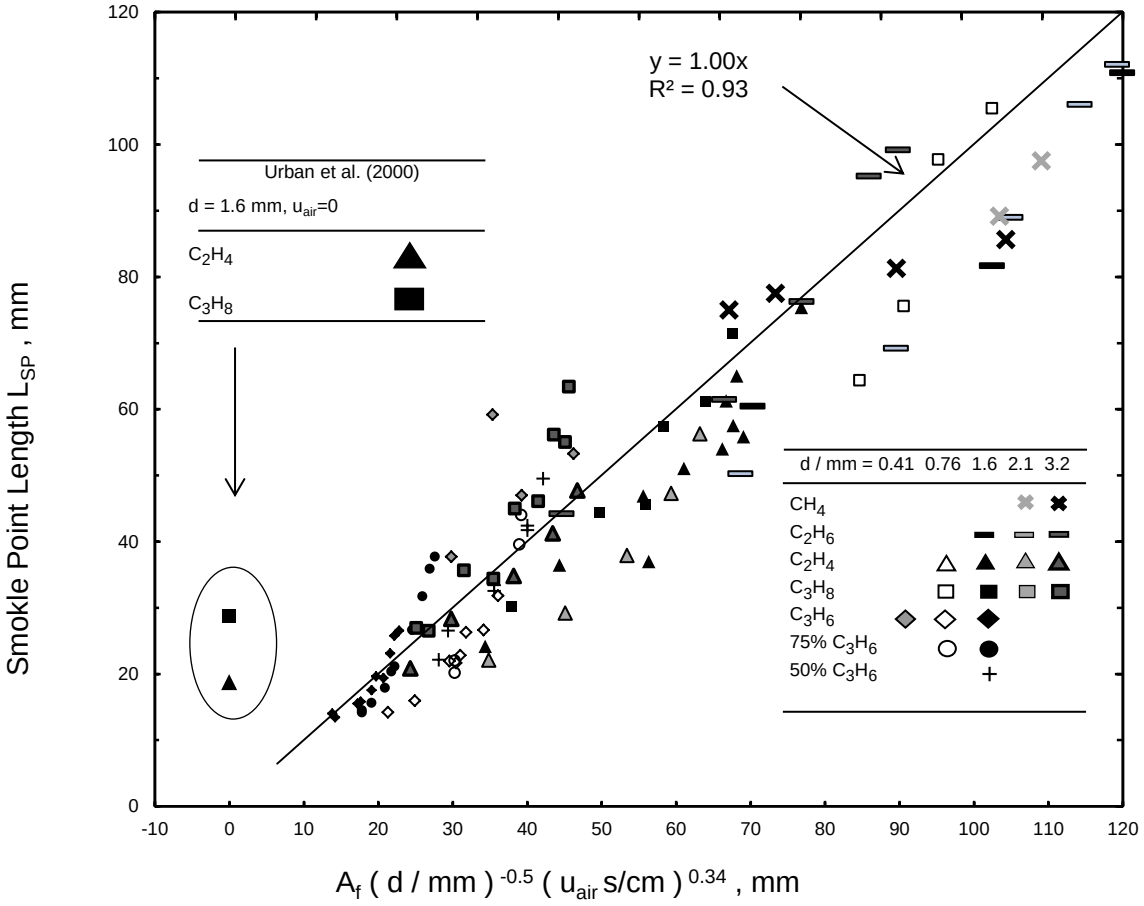

Figure 3.16: Smoke point flame length and scaled correlation. All of the data found from the MSG was used to update the correlation. Ethylene at the 0.76 mm burner not included in this plot.

injection velocity from the 3.2 mm burner to the 2.1 mm burner increased by a factor of two. In the transition from the 1.6 mm to the 0.76 mm burner the fuel velocity increased by a factor of six. At the 1.6 mm burner the difference of injection velocities of ethylene and propane is 40.78 cm/s-115 cm/s and 39.24-64.46 cm/s respectively. When switching to the 0.76 mm burner the injection velocity of ethylene and propane increases to 551.07-714.21 cm/s and 330.64-389.1 cm/s. The difference in the change in injection

velocities as the burner diameter is minimized could account for the switch in sooting propensity. Propane's injection velocity is always smaller than ethylene but when switching to the 0.76 mm burner the difference is 325 cm/s instead of around 50.5 cm/s for the 1.6mm burner. The large difference in the injection velocity of the propane and ethylene at the 0.76 mm burner gives propane a larger amount of time in the soot formation region. Dotson did work to measure these residence times but the results were inconclusive. Extensive research on residence times will provide some more differences between the 0.76 mm and 1.6 mm burners.

The change in the correlation shows a few new thoughts about the contributors on smoke points in microgravity. While burner size and diameter are still a dominating factor in the smoke point length, it is not as pronounced as originally thought. The effect of coflow decreased from 0.412 to 0.272 and the effect of burner size decreased from -0.91 to -0.665. Both of the factors were scaled down by closely equivalent amounts with coflow being scaled down slightly more. The decrease in the exponents of the correlation was counteracted by the increase in fuel factors. The fuel factors all increased by around thirty percent. The type of fuel is a larger factor in the smoke point length than in the original correlation. The fuel should be a large factor in the correlation because molecular shape has a large effect on a fuels sooting propensity. A fuel like propane is cleaner burning than the double bonded propylene. According to A_f values, propylene (10.37) is more likely to produce soot than propane (32.88). The same is true for ethylene and ethane. Ethylene (34.8) is more likely to produce soot than ethane (64.92). Relating these fuel factors to a flame's actual soot production would be the next step. Further testing would need to be done to find out how much more an A_f value

of 20 is to a value of 40. This kind of testing could be done through smoke sampling of burning flames. The smoke point length is dominated by the fuel type and modified by coflow velocity and burner size.

The correlation was thought up based on the controlling factors of the experiment. There correlation was created because the dependence on one factor other than mass flow rate could not be found. Mass flow rate dependence, seen in Figure 3.17, is expected because of its relationship with smoke point length. This high R^2 doesn't provide any explanation into smoke point lengths and their existence. Many different approaches were tried for finding meaningful smoke point length plots. Residence times were examined in Dotson's work without the result of quantitative correlations. Radiative losses of the flames were measured but those measurements were not reliable. Mass flow rate over stoichiometric mixture fractions were examined as well in Dotson's work [38]. Further work on residence times and radiative loss fractions could provide some insight on the controlling mechanisms of soot formation. The difficulty in finding quantitative correlations for the smoke point length suggests that there may be multiple contributing factors. The next step would be to find the level of contribution of these factors. The four common smoke point explanations are: a smoke point occurs when the soot temperature reaches its critical temperature of 1300 K (1000 K for microgravity) before its burnout; a smoke point occurs when the radiative loss fraction increases until it reaches 0.2-0.4 for normal gravity or 0.4-0.6 for microgravity; a smoke point occurs when the ratio of the luminous length and the stoichiometric length increase with increased fuel flow until it reaches a smoke point around two; a smoke point occurs when the increase in flame residence time also increases the time available for soot

formation and oxidation. The definitions were discussed earlier as not being mutually exclusive. There may be contributions from a number of factors discussed.

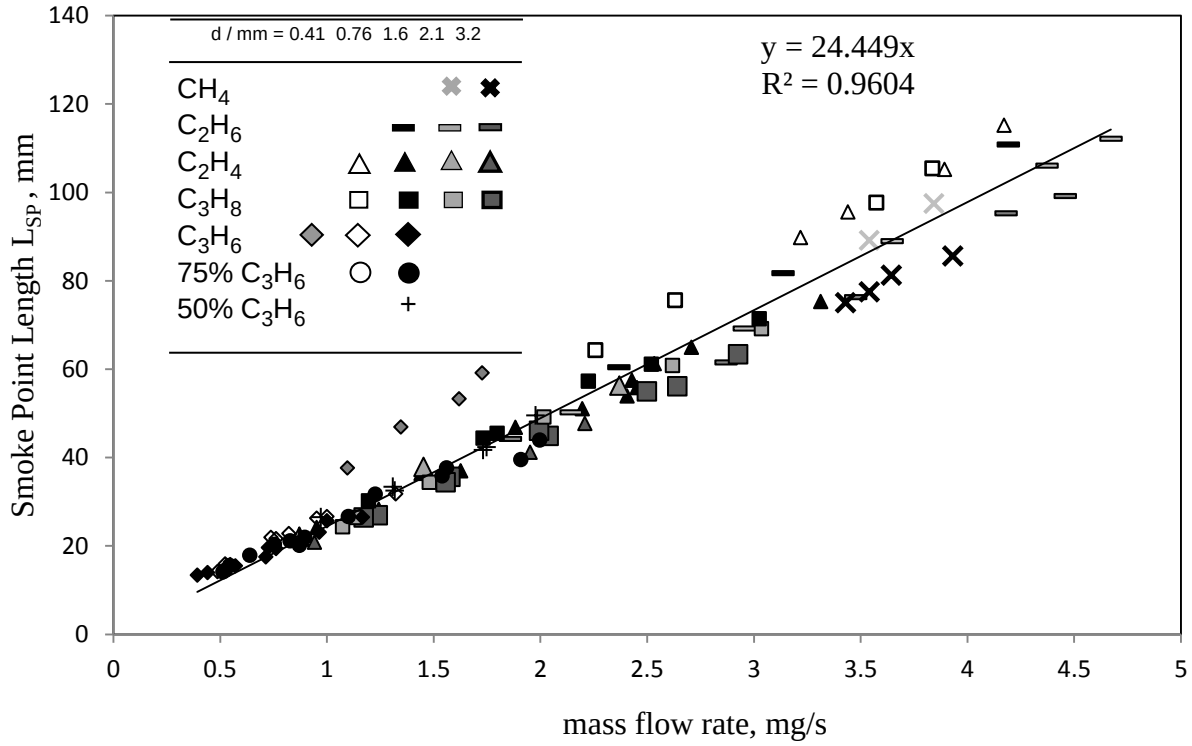

Figure 3.17: Smoke point flame length against the mass flow rate of the given fuel.

3.5 Procedures

The procedure is something that needs to be called into question when examining smoke points in microgravity. It is important to remove any unnecessary source of error in the data. The largest source of error that can come from these studies is the difference of interpretation of a smoke point. The difference between a smoking and non-smoking condition is not difficult to view, but is made more challenging when watching a recording of the tests. The astronaut has a firsthand view of the smoking condition where

the people on the ground do not. Smoke points that are observed and indicated by the astronaut or whoever has a firsthand view of the experiment will reduce the error associated with the smoke points. The person with a firsthand view of the experiment can explicitly see whether the flame is smoking or not.

It is more difficult to see smoke in the video version of the test. This may be due to the quality of the video camera and an update in equipment would be beneficial. The smoke point is the transition from smoking to non-smoking flame so small amounts of smoke need to be observed. An astronaut better trained in what a smoke point condition is would provide the best results. Towards the middle of the study the astronaut started to indicate when the smoke point condition occurred with at shoulder movement. This visual movement took away any ambiguity of when the flame was at its transition point. Other visual cues, like an LED light, would be beneficial in the flame's video. There should also be a standard way of finding a smoke point condition. The clearest tests were when the flame was brought past the smoke point and the fuel was slowly decreased until a smoke point was reached. When approached from a smoking flame the transition is more distinctive. Some of the tests were approached from the nonsmoking side and the transition was not reached. Each data point is very important due to the environment it takes to recreate the data.

Chapter 4 Conclusions

Microgravity smoke points of four different fuels were observed. Methane, ethane, ethylene, and propane were observed with varying burner sizes of 0.76, 1.6, 2.1, and 3.2 mm. A total of 57 smoke points were found to double the previous study of 55 smoke points to expand to 112 smoke points total. Previous work by Dotson emphasized the relationship of microgravity smoke point length with burner size and coflow velocity. Decreasing the burner diameter will increase the smoke point length. Increasing the coflow velocity will increase the smoke point length. The increase in smoke point lengths can be attributed to the change in residence times in the soot formation and soot oxidation region. The increase in coflow velocities and reduction in burner diameter can cause the soot volume fraction profile to shift downstream creating a longer smoke point length. Previous work on residence time and soot formation time to soot oxidation time ratio did not provide any relation between residence time and smoke points and was not evaluated for the new data.

With the previous smoke point data collected by Dotson, the fuel sooting propensity are shown as follows: methane < ethane < ethylene < propane < 50% propylene < 75% propylene < propylene. The ranking is based on the A_f values found for the fuels, which can be found in Table 3.1. There is an exception in the 0.76 mm burner for ethylene and propane. Propane produces less soot than ethylene in the 3.2, 2.1, and 1.6 mm, but ethylene is less sooty than propane in the 0.76 mm burner. This is contrary to normal gravity studies where sooting propensity is as follows: methane < ethane < propane < ethylene < 50% propylene < 75% propylene < propylene. In normal

gravity the propane fuel produces less soot in all cases. The switch in sooting characteristics from the 1.6 to 0.76 mm burn could be a result of the fuel injection velocity. The fuel injection velocity increases more in the change from the 1.6 to the 0.76 mm burner than any other burner change. The increase is so substantial that it could account for the switch in sooting characteristics of the flames. Further testing could be done to validate this effect. Similar fuel pairings to the ethylene/propane pairing could be used to study this velocity effect. The important factor to consider is what the 0.76 mm burner and high injection velocities do to the fuels being studied.

Previously microgravity smoke points were scaled in the form $L_{SP} = A_f d^a u_{air}^b$, with a= - 0.910 *b*= 0.414. Given the work in the present study and the previous scaling equation $L_{SP} = A_f d^a u_{air}^b$, a and b were updated to a = -0.665 and 0.272. The updated correlation involves two new fuels and 57 additional smoke points. The new correlation comes with new fuel factors (A_f). The A_f values are increased by approximately 30 percent of the originally derived factors. The increase in A_f values and decrease in a and b values shows a greater dependence on the particular fuel type than previously found. The a and b values decreasing show that their effect is less pronounced than originally thought. However, the ratio of burner size and coflow velocity effect was very similar, but each was scaled down. Even though the burner diameter and coflow velocity decreased that does not diminish their effect. The two parameters are still controlling factors in the length of the smoke point.

Methane smoke points were found for the first time at normal pressures. Since methane produces less soot than other fuels, its smoke point is too long for normal gravity tests. Methane's simple structure makes it difficult to decompose into acetylene.

The methane smoke points nearly reached the edge of the field of view in the MSG with coflow velocities up to 15.51 cm/s. Where in tests of other fuels in microgravity, coflow velocities of up to 65 cm/s were used. With the addition of methane smoke points, methane flames can be compared with the sooting of other fuels when it previously could not.

This study does not prove the cause of smoke points or distinguish which of the four commonly used mechanisms is dominant. This study provides fundamental data set that can be used in CFD soot models. It has updated original correlations for smoke point length correlations. A total of 57 smoke points were found to double the previous study of 55 smoke points to expand to 112 smoke points total. Methane and ethane were two new fuels observed, leading to the first standard pressure methane smoke points. There were hopes in the experimentation to find the radiative losses at the smoke point condition, but the data was not reliable. The results of the study will hopefully lead to a better idea of smoke points and lead to further experiments distinguishing the dominant mechanisms in sooting flames.

Chapter 5 Appendices

5.1 Microgravity Smoke Point Results

Fuel	Nozzle (mm)	GMT	Author	Time Observed	Fuel Velocity (cm/s)	Flow Rate (mg/s)	Coflow Velocity (cm/s)	Length (mm)	Reynolds Number
Methane	3.2	72	DeBold	10:46:22	66.25	3.47	4.20	77.50	127.89
Methane	3.2	72	DeBold	10:46:52	64.16	3.36	3.02	75.00	123.86
Methane	3.2	72	DeBold	10:47:21	68.19	3.57	8.83	81.25	131.63
Methane	3.2	72	DeBold	10:48:09	73.56	3.85	15.51	85.63	142.00
Methane	2.1	72	DeBold	10:58:14	153.83	3.47	5.37	89.17	194.88
Methane	2.1	72	DeBold	10:58:40	166.99	3.77	6.53	97.50	211.560
Ethane	3.2	69	DeBold	12:45:41	19.89	1.95	3.02	44.17	94.67
Ethane	3.2	69	DeBold	12:46:33	27.87	2.74	13.32	61.46	132.64
Ethane	3.2	69	DeBold	12:47:26	33.78	3.32	22.91	76.25	160.74
Ethane	3.2	69	DeBold	12:48:06	40.62	3.99	34.59	95.21	193.28
Ethane	3.2	69	DeBold	12:48:44	43.31	4.25	40.81	99.17	206.10
Ethane	2.1	69	DeBold	13:08:23	48.36	2.04	5.37	50.21	151.02

Ethane	2.1	69	DeBold	13:08:57	66.65	2.82	14.42	69.17	208.12
Ethane	2.1	69	DeBold	13:09:34	82.28	3.48	25.95	88.96	256.95
Ethane	2.1	69	DeBold	13:10:09	98.64	4.17	35.50	106.04	308.05
Ethane	2.1	69	DeBold	13:10:31	105.38	4.45	41.67	112.08	329.09
Ethane	1.6	69	DeBold	14:22:15	92.01	2.26	3.02	60.42	218.92
Ethane	1.6	69	DeBold	14:23:00	121.85	2.99	12.21	81.67	289.92
Ethane	1.6	69	DeBold	14:23:36	162.89	4.00	21.88	110.83	387.55
Ethylene	3.2	83	DeBold	11:35:21	10.07	0.92	3.02	20.83	36.60
Ethylene	3.2	83	DeBold	11:35:48	13.30	1.22	6.53	28.33	48.35
Ethylene	3.2	83	DeBold	11:36:10	16.66	1.53	16.60	34.79	60.56
Ethylene	3.2	83	DeBold	11:36:31	20.89	1.91	26.94	41.25	75.92
Ethylene	3.2	83	DeBold	11:36:50	23.62	2.16	35.50	47.71	85.86
Ethylene	2.1	83	DeBold	11:06:29	21.65	0.85	4.20	22.08	51.65
Ethylene	2.1	83	DeBold	11:07:01	29.74	1.17	11.09	29.17	70.93
Ethylene	2.1	83	DeBold	11:07:34	38.98	1.54	20.84	37.92	86.08
Ethylene	2.1	83	DeBold	11:07:59	51.39	2.03	30.83	47.29	118.44

Ethylene	2.1	83	DeBold	11:08:32	58.90	2.32	39.08	56.25	140.48
Ethylene	1.6	83	DeBold	11:53:25	40.78	0.93	3.02	24.17	74.11
Ethylene	1.6	83	DeBold	11:53:45	61.67	1.41	7.68	36.46	112.07
Ethylene	1.6	83	DeBold	11:54:10	80.57	1.85	17.67	46.88	146.41
Ethylene	1.6	83	DeBold	11:54:31	94.00	2.15	24.94	51.04	170.82
Ethylene	1.6	83	DeBold	11:54:56	108.42	2.48	34.59	61.25	197.03
Ethylene	1.6	83	DeBold	11:55:12	115.88	2.65	37.31	65.00	210.59
Ethylene	1.6	45	Dotson	15:00:23	141.71	3.31	58.02	75.35	257.55
Ethylene	1.6	45	Dotson	14:37:08	102.93	2.41	33.57	53.99	187.07
Ethylene	1.6	45	Dotson	14:50:07	104.92	2.45	39.21	55.83	190.68
Ethylene	1.6	168	Dotson	9:49:13	103.92	2.43	36.39	57.50	188.87
Ethylene	1.6	45	Dotson	15:48:39	69.61	1.63	18.53	36.99	126.52
Ethylene	0.76	83	DeBold	12:18:08	551.07	3.16	3.02	89.79	527.07
Ethylene	0.76	83	DeBold	12:18:27	588.87	3.37	6.53	95.63	563.22
Ethylene	0.76	83	DeBold	12:19:00	714.21	4.09	18.74	115.21	683.09
Ethylene	0.76	45	Dotson	17:28:29	734.59	3.89	17.59	105.22	635.76

Propane	3.2	72	DeBold	14:35:31	8.43	1.21	4.20	26.92	60.62
Propane	3.2	72	DeBold	14:35:55	10.74	1.55	9.96	35.62	77.25
Propane	3.2	72	DeBold	14:36:18	13.88	2.00	20.84	44.94	99.77
Propane	3.2	72	DeBold	14:36:48	17.98	2.59	33.66	56.12	129.28
Propane	3.2	72	DeBold	14:37:15	19.92	2.87	39.95	63.37	143.23
Propane	3.2	55	DeBold	12:53:15	7.98	1.15	5.37	26.46	57.40
Propane	3.2	55	DeBold	12:53:57	10.59	1.53	15.51	34.38	76.17
Propane	3.2	55	DeBold	12:57:12	13.58	1.96	27.93	46.04	97.63
Propane	3.2	55	DeBold	12:58:12	17.01	2.45	38.20	55.00	122.30
Propane	2.1	72	DeBold	14:44:56	16.98	1.05	5.37	26.46	84.19
Propane	2.1	55	DeBold	11:52:58	16.98	1.05	4.20	24.38	80.11
Propane	2.1	55	DeBold	11:56:33	23.39	1.45	15.51	34.38	110.35
Propane	2.1	55	DeBold	12:08:09	33.61	2.08	25.95	49.17	150.40
Propane	2.1	55	DeBold	12:09:08	41.40	2.57	38.20	60.83	195.36
Propane	2.1	55	DeBold	12:11:57	47.98	2.98	46.61	69.17	226.42
Propane	1.6	55	DeBold	15:12:23	32.53	1.17	5.37	30.21	116.94

Propane	1.6	55	DeBold	15:13:13	48.04	1.73	14.42	44.38	169.51
Propane	1.6	55	DeBold	15:14:00	64.46	2.32	25.95	57.29	217.78
Propane	1.6	48	Dotson	16:54:27	82.34	3.03	44.85	71.38	296.07
Propane	1.6	48	Dotson	17:12:08	68.62	2.52	36.39	61.12	246.72
Propane	1.6	48	Dotson	17:45:17	48.93	1.80	22.29	45.52	175.93
Propane	0.76	55	DeBold	15:36:51	389.13	3.50	28.91	97.71	736.31
Propane	0.76	52	Dotson	11:39:28	460.49	3.84	33.57	105.45	788.45
Propane	0.76	52	Dotson	11:43:05	315.76	2.63	21.35	75.58	540.65
Propane	0.76	52	Dotson	11:49:43	271.03	2.26	16.65	64.33	464.06
50% Propylene	1.6	55	Dotson	9:40:13	98.80	2.89	40.15	41.73	181.04
50% Propylene	1.6	55	Dotson	9:37:29	75.18	2.20	26.05	32.50	137.77
50% Propylene	1.6	167	Dotson	9:23:36	55.42	1.62	12.89	26.52	101.56
50% Propylene	1.6	167	Dotson	9:32:48	74.70	2.18	26.05	33.41	136.89
50% Propylene	1.6	167	Dotson	9:41:01	99.76	2.91	40.15	42.38	182.81
50% Propylene	1.6	167	Dotson	9:45:36	112.78	3.29	48.61	49.51	206.66
50% Propylene	1.6	55	Dotson	8:56:28	49.64	1.45	11.01	22.12	90.96

75% Propylene	1.6	52	Dotson	16:14:10	59.39	1.91	64.60	37.68	144.12
75% Propylene	1.6	173	Dotson	10:38:23	58.59	1.88	58.96	35.84	142.18
75% Propylene	1.6	52	Dotson	16:26:48	46.63	1.50	51.43	31.70	113.17
75% Propylene	1.6	173	Dotson	11:09:27	41.85	1.34	42.03	26.65	101.57
75% Propylene	1.6	52	Dotson	16:23:20	31.49	1.01	28.87	21.14	76.41
75% Propylene	1.6	52	Dotson	16:09:59	19.93	0.64	12.89	14.47	48.36
75% Propylene	1.6	119	Dotson	10:29:30	19.53	0.63	12.89	14.16	47.39
75% Propylene	1.6	119	Dotson	10:38:53	28.70	0.92	26.99	20.36	69.64
75% Propylene	1.6	136	Dotson	15:57:52	20.73	0.67	16.65	15.61	50.30
75% Propylene	1.6	136	Dotson	15:53:36	24.31	0.78	23.23	17.88	59.00
75% Propylene	0.76	52	Dotson	17:30:19	261.89	1.91	37.33	39.52	302.65
75% Propylene	0.76	136	Dotson	17:23:30	123.04	0.90	14.77	21.97	142.18
75% Propylene	0.76	136	Dotson	17:21:52	119.52	0.87	14.77	20.15	138.12
75% Propylene	0.76	173	Dotson	12:40:44	274.20	2.00	38.27	43.98	316.86
Propylene	1.6	58	Dotson	9:55:18	28.54	1.00	51.43	25.73	92.72
Propylene	1.6	58	Dotson	9:47:05	20.73	0.73	33.57	19.63	67.33

Propylene	1.6	58	Dotson	9:44:17	15.63	0.55	22.29	15.79	50.77
Propylene	1.6	58	Dotson	9:37:52	12.57	0.44	9.13	13.99	40.84
Propylene	1.6	174	Dotson	10:45:25	16.31	0.57	20.41	15.49	52.98
Propylene	1.6	174	Dotson	10:48:31	11.21	0.39	10.07	13.42	36.42
Propylene	1.6	174	Dotson	11:04:43	20.39	0.71	29.81	17.56	66.23
Propylene	1.6	174	Dotson	11:13:17	33.30	1.17	57.08	26.53	108.17
Propylene	1.6	174	Dotson	11:20:47	27.52	0.96	46.73	23.08	89.41
Propylene	1.6	174	Dotson	11:24:30	21.75	0.76	40.15	19.40	70.65
Propylene	0.76	58	Dotson	10:41:14	125.87	1.00	41.09	26.63	194.71
Propylene	0.76	58	Dotson	10:36:19	103.39	0.82	28.87	22.80	159.94
Propylene	0.76	58	Dotson	12:45:46	95.90	0.76	26.99	21.67	148.35
Propylene	0.76	174	Dotson	12:34:00	92.90	0.74	24.17	21.93	143.71
Propylene	0.76	174	Dotson	12:36:12	65.93	0.52	12.89	15.95	101.99
Propylene	0.76	174	Dotson	12:43:03	166.32	1.32	50.49	31.82	257.29
Propylene	0.76	174	Dotson	12:46:17	119.87	0.95	31.69	26.30	185.43
Propylene	0.76	58	Dotson	10:13:22	61.44	0.49	7.24	14.21	95.03

Propylene	0.41	58	Dotson	11:32:00	716.43	1.62	26.99	53.28	591.08
Propylene	0.41	58	Dotson	11:25:49	595.27	1.35	14.77	46.96	491.12
Propylene	0.41	174	Dotson	11:46:06	763.84	1.73	10.07	59.19	630.20
Propylene	0.41	58	Dotson	11:23:08	484.64	1.10	5.36	37.70	399.85

5.2 Flame Images and Information

Fuel	C_3H_8	C_3H_8	C_3H_8	C_3H_8	C_3H_8
Nozzle	3.2	3.2	3.2	3.2	3.2
GMT	079	079	079	079	079
Time	14:35:31	14:35:55	14:36:18	14:36:48	14:37:15
Air (cm/s)	4.20	9.96	20.84	33.65	39.94
Length (mm)	26.92	35.62	44.94	56.12	63.37

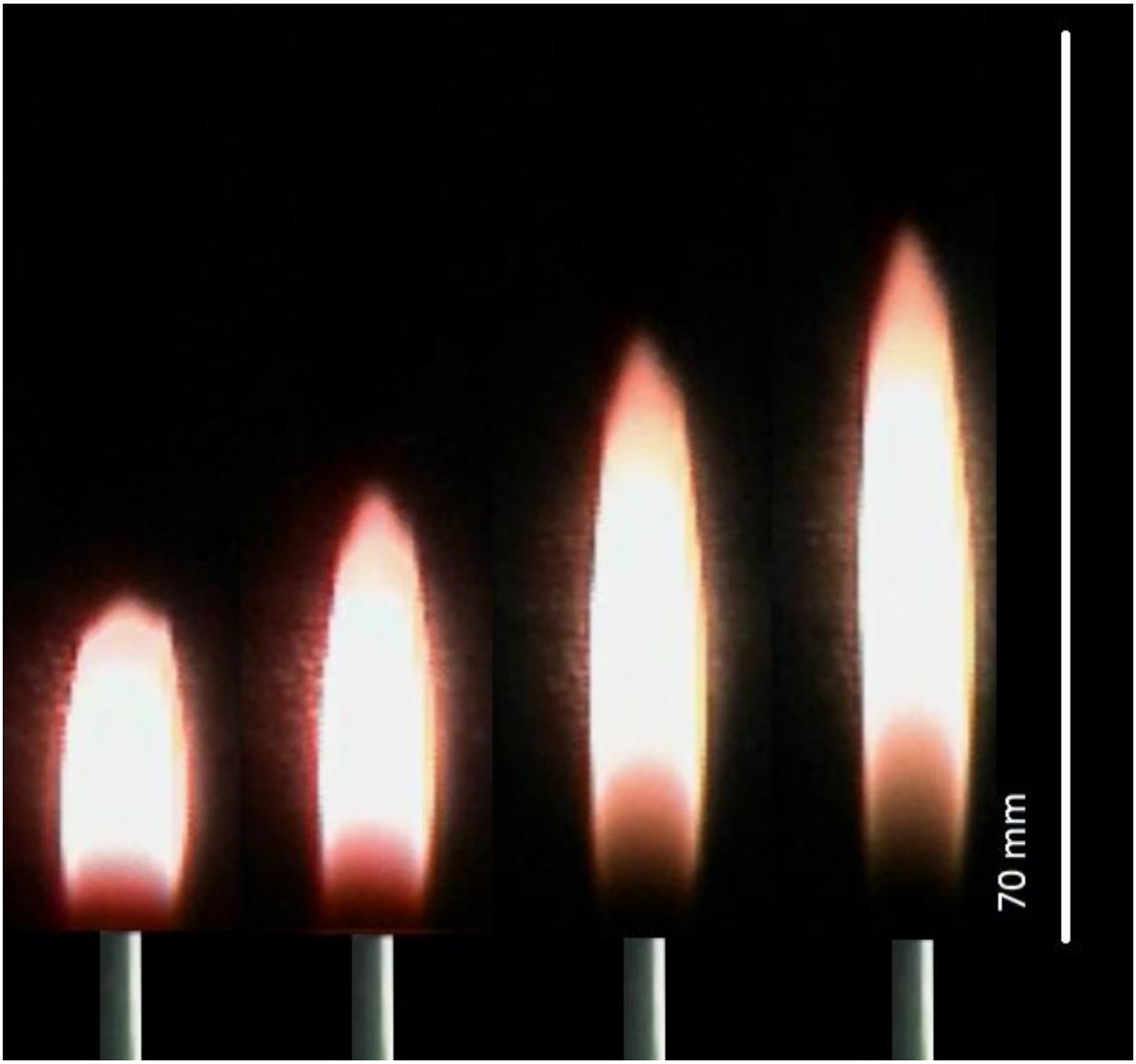

Fuel	C_3H_8	C_3H_8	C_3H_8	C_3H_8
Nozzle	3.2	3.2	3.2	3.2
GMT	055	055	055	055
Time	12:53:15	12:53:57	12:57:12	12:58:12
Air (cm/s)	5.37	15.51	27.93	38.20
Length (mm)	26.46	34.38	46.04	55

Fuel	C_3H_8	C_3H_8	C_3H_8	C_3H_8	C_3H_8	C_3H_8
Nozzle	2.1	2.1	2.1	2.1	2.1	2.1
GMT	055	079	055	055	055	055
Time	11:52:58	14:44:56	11:56:33	12:08:09	12:09:08	12:11:57
Air (cm/s)	4.20	5.37	15.51	25.95	38.20	46.61
Length (mm)	26.46	24.38	34.38	49.17	60.83	69.17

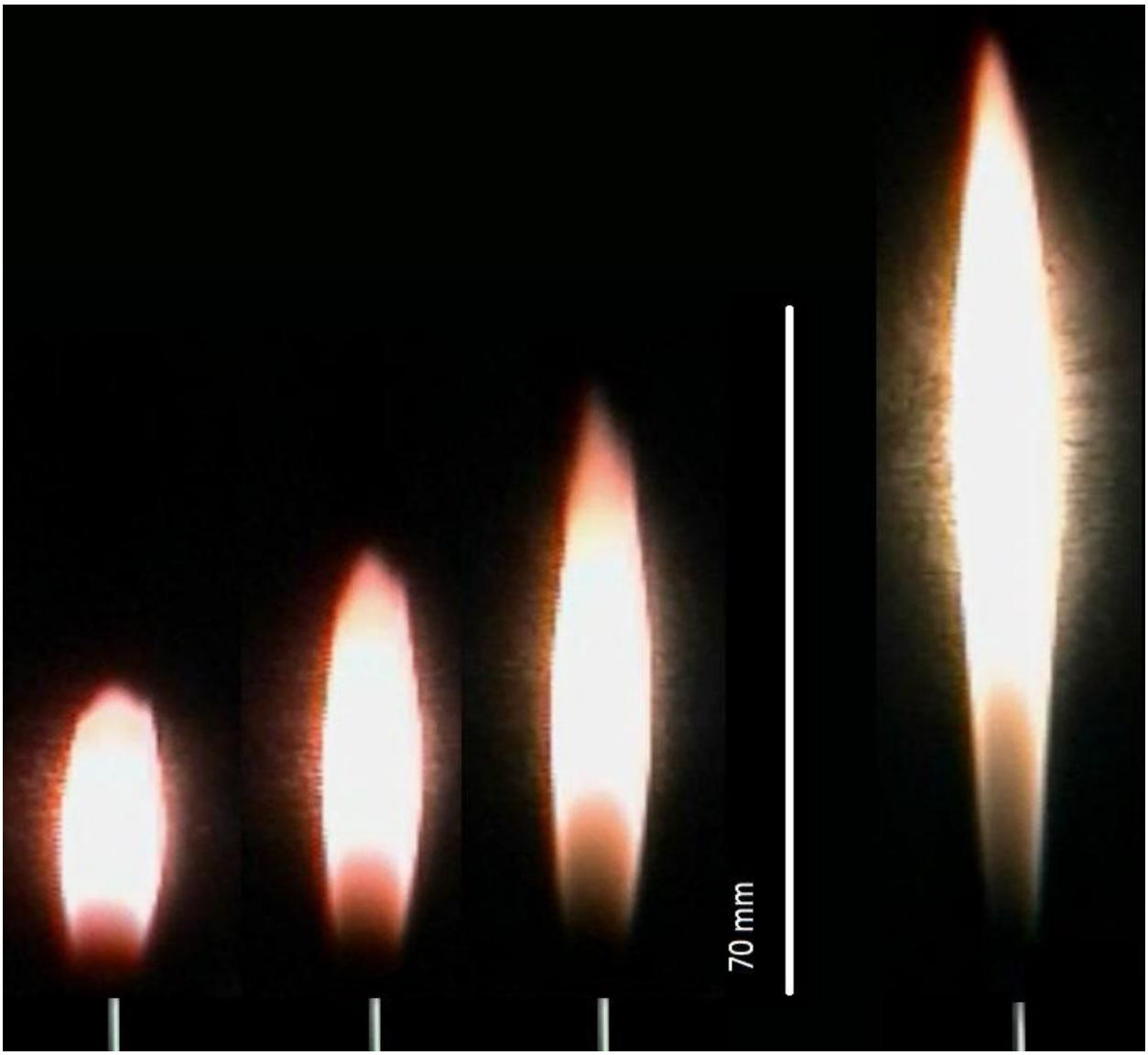

Fuel	C_3H_8	C_3H_8	C_3H_8	C_3H_8
Nozzle	1.6	1.6	1.6	0.76
GMT	055	055	055	055
Time	15:12:23	15:13:13	15:14:00	15:36:51
Air (cm/s)	5.37	14.42	25.95	28.91
Length (mm)	30.21	44.38	57.29	97.71

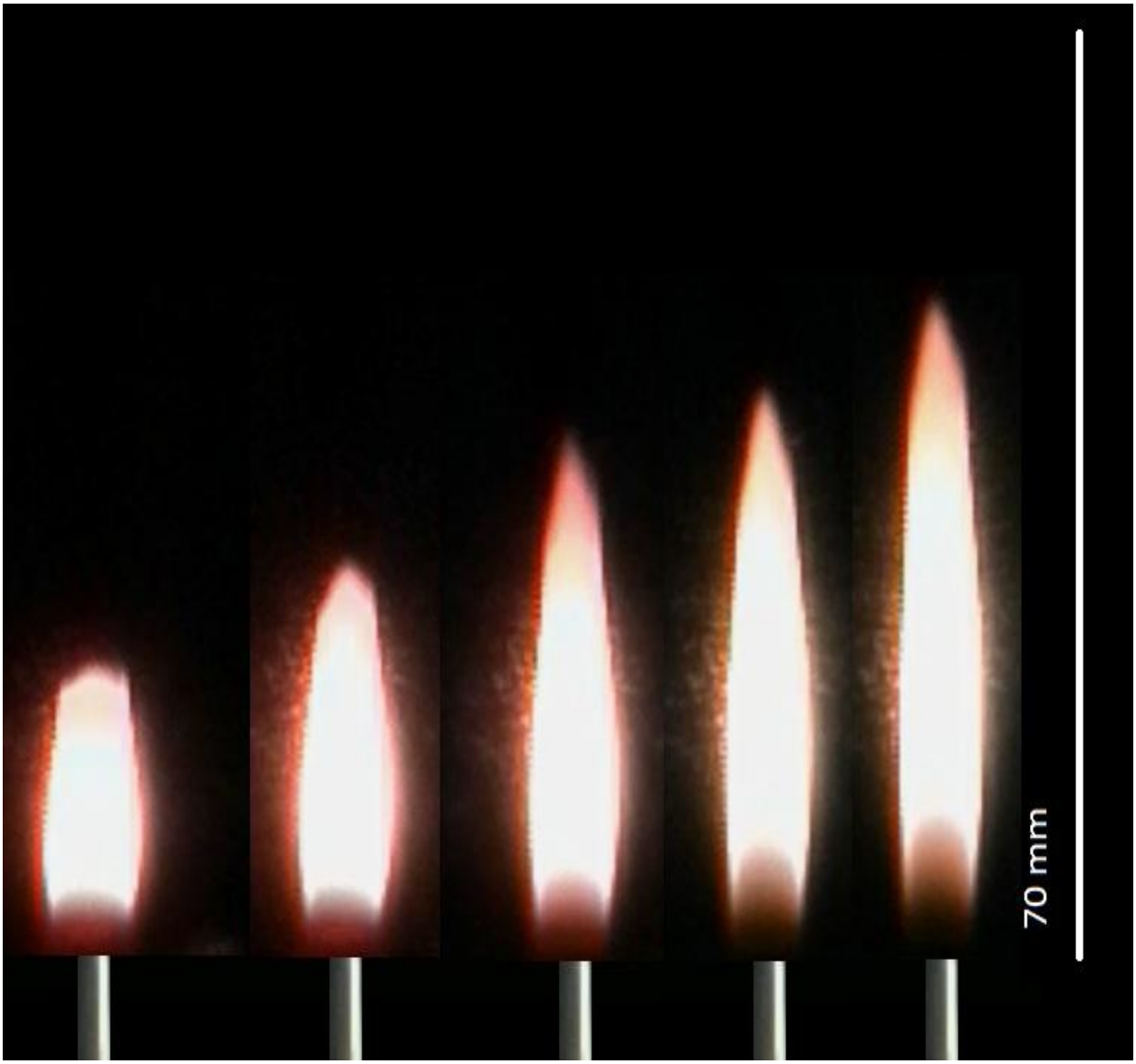

Fuel	C_2H_4	C_2H_4	C_2H_4	C_2H_4	C_2H_4
Nozzle	3.2	3.2	3.2	3.2	3.2
GMT	083	083	083	083	083
Time	11:35:19	11:35:48	11:36:10	11:36:31	11:36:50
Air (cm/s)	3.02	6.53	16.60	26.94	35.50
Length(mm)	20.83	28.33	34.79	41.25	47.71

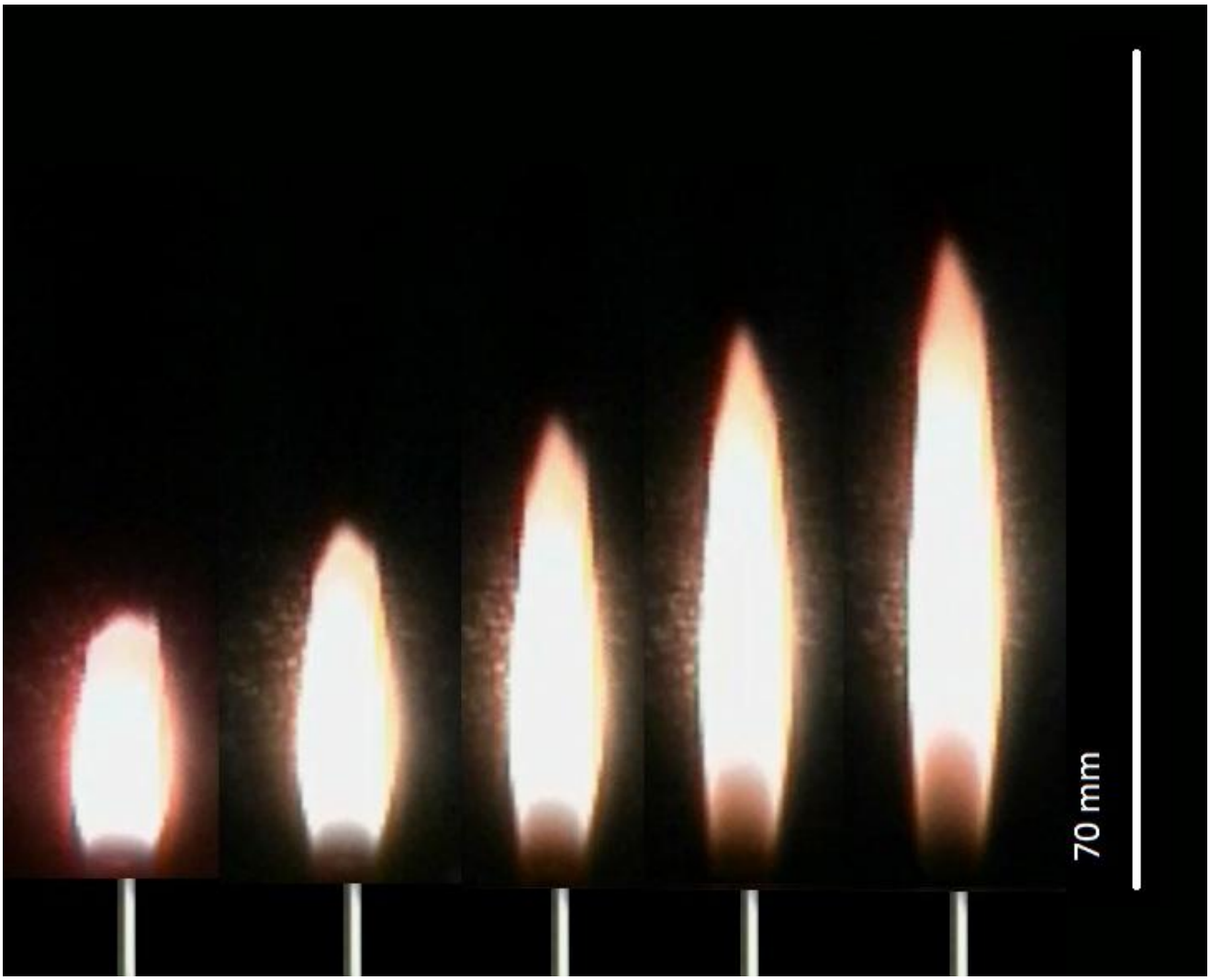

Fuel	C_2H_4	C_2H_4	C_2H_4	C_2H_4	C_2H_4
Nozzle	2.1	2.1	2.1	2.1	2.1
GMT	083	083	083	083	083
Time	11:06:29	11:07:01	11:07:34	11:07:59	11:08:32
Air (cm/s)	4.20	11.09	20.84	30.83	39.08
Length (mm)	22.08	29.17	37.92	47.29	56.25

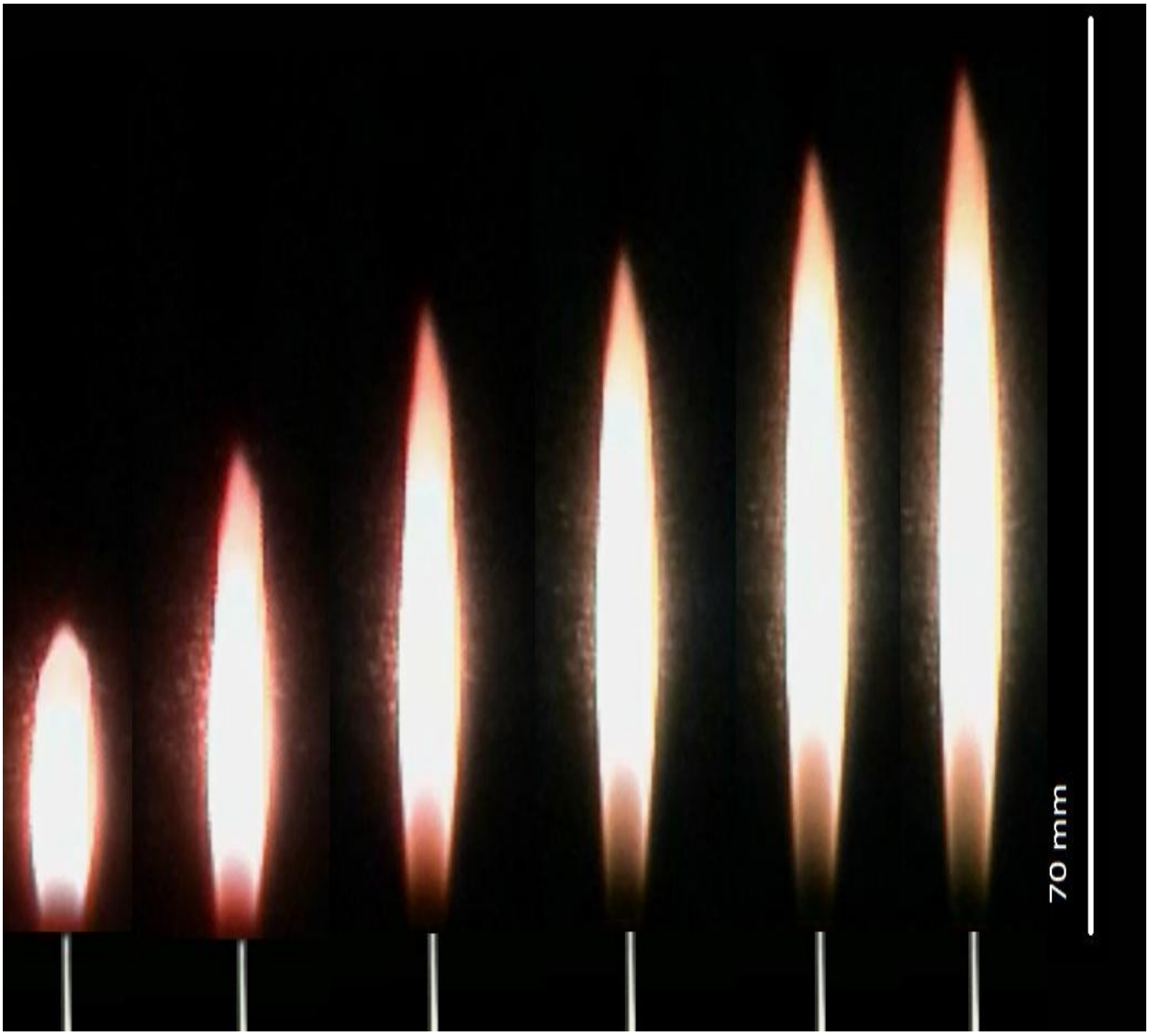

Fuel	C_2H_4	C_2H_4	C_2H_4	C_2H_4	C_2H_4	C_2H_4
Nozzle	1.6	1.6	1.6	1.6	1.6	1.6
GMT	083	083	083	083	083	083
Time	11:53:25	11:53:45	11:54:10	11:54:31	11:54:56	11:55:12
Air (cm/s)	3.02	7.68	17.67	24.94	34.59	37.31
Length (mm)	24.17	36.46	46.88	51.04	61.25	65

Fuel	C_2H_4	C_2H_4	C_2H_4
Nozzle	0.76	0.76	0.76
GMT	083	083	083
Time	12:18:08	12:18:27	12:19:00
Air (cm/s)	3.02	6.53	18.74
Length (mm)	89.79	95.63	115.21

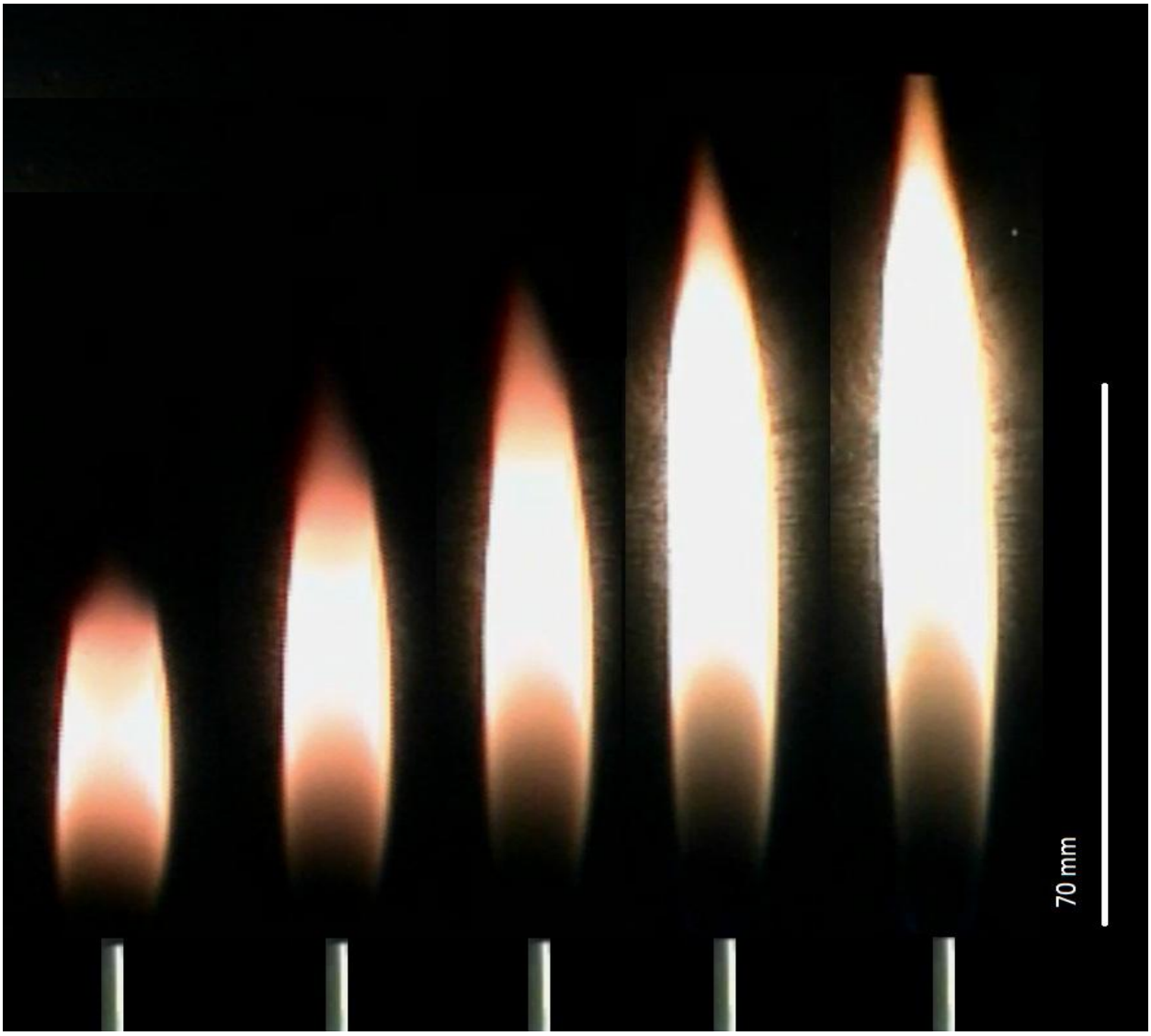

Fuel	C_2H_6	C_2H_6	C_2H_6	C_2H_6	C_2H_6
Nozzle	3.2	3.2	3.2	3.2	3.2
GMT	069	069	069	069	069
Time	12:45:41	12:46:33	12:47:26	12:48:06	12:48:44
Air (cm/s)	3.02	13.32	22.91	34.59	40.81
Length (mm)	44.17	61.46	76.25	95.21	99.17

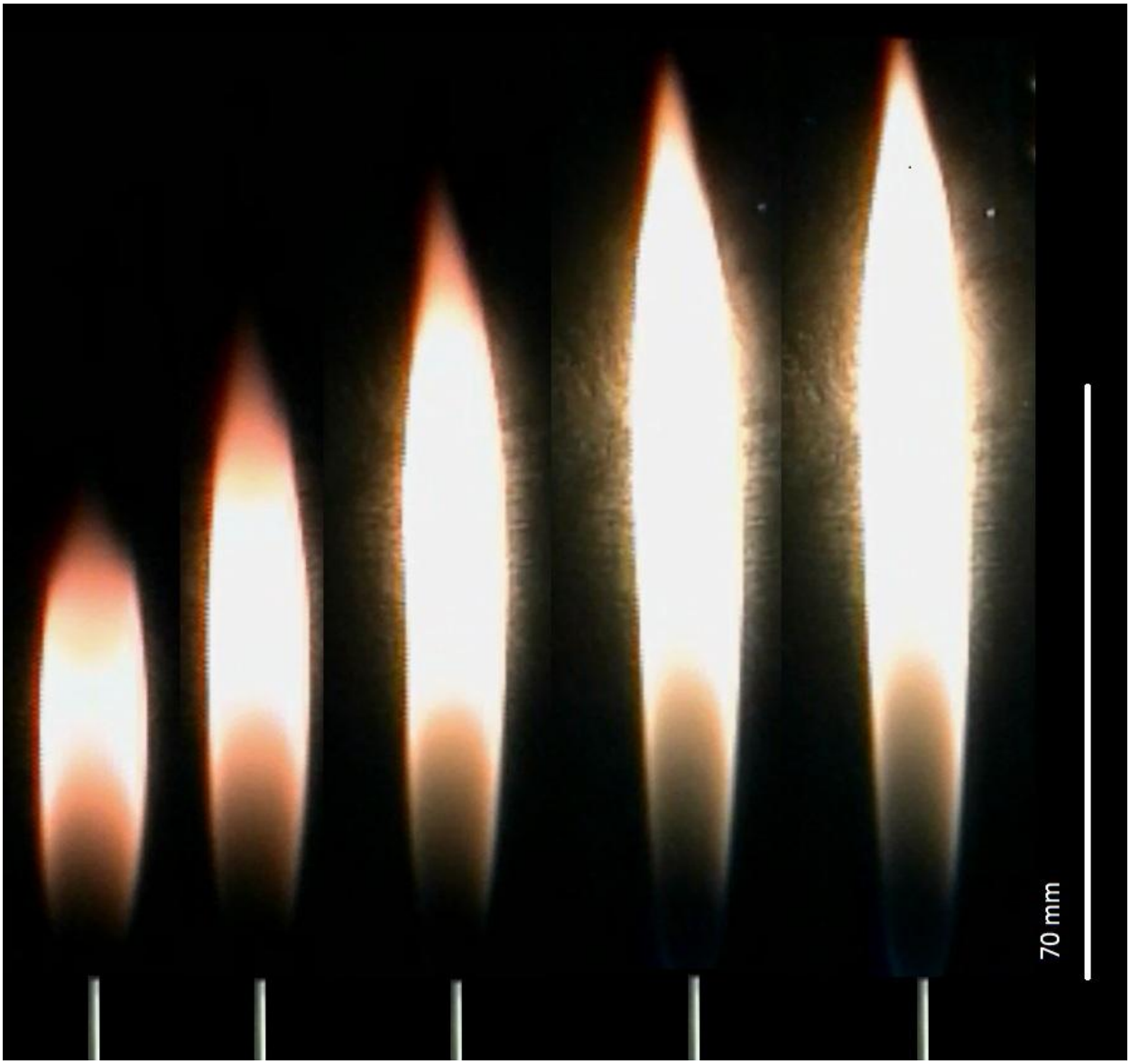

Fuel	C_2H_6	C_2H_6	C_2H_6	C_2H_6	C_2H_6
Nozzle	2.1	2.1	2.1	2.1	2.1
GMT	069	069	069	069	069
Time	13:08:23	13:08:57	13:09:34	13:10:09	13:10:31
Air (cm/s)	5.37	14.42	25.95	35.50	41.67
Length (mm)	50.21	69.17	88.96	106.04	112.08

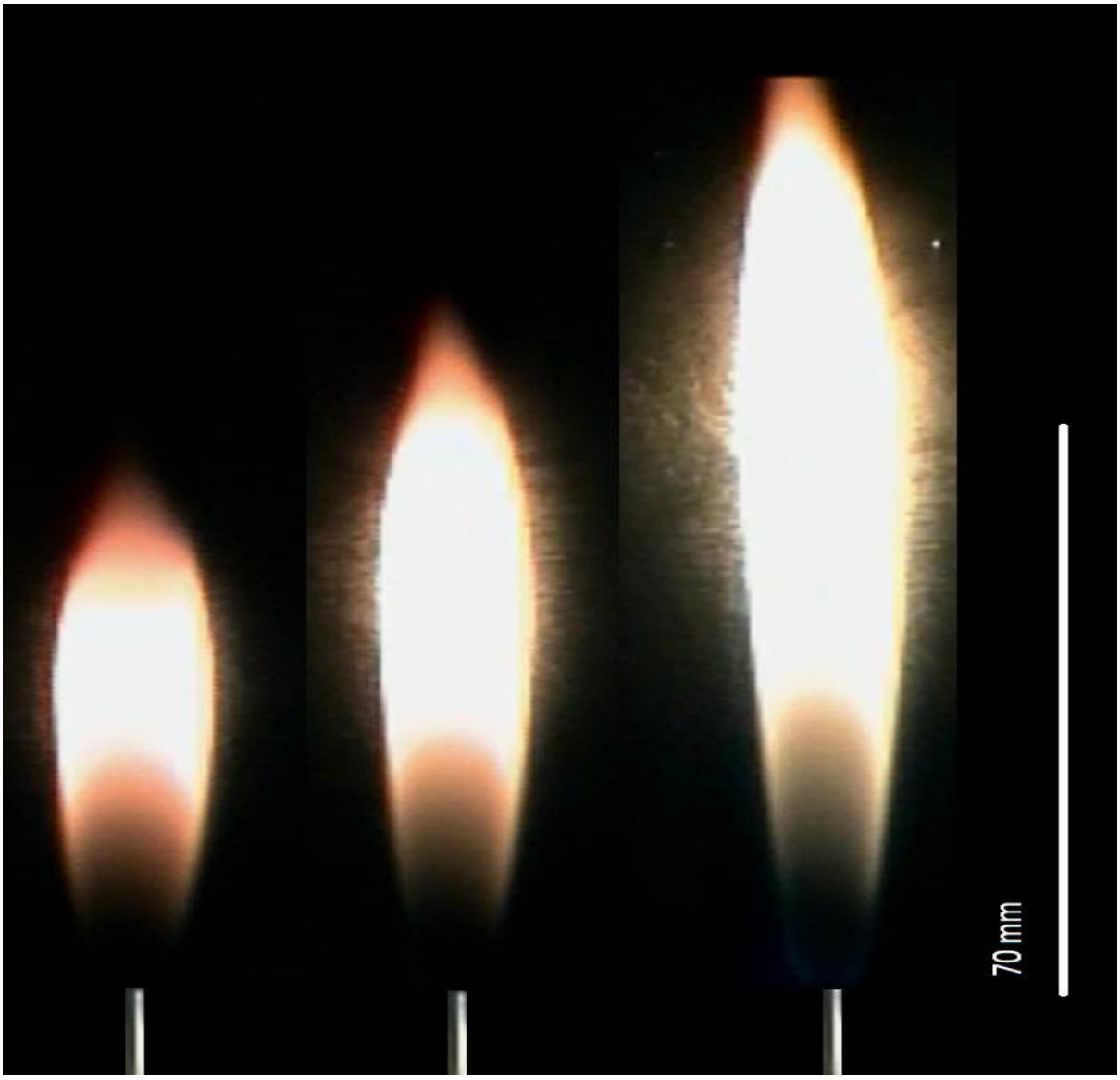

Fuel	C_2H_6	C_2H_6	C_2H_6
Nozzle	1.6	1.6	1.6
GMT	069	069	069
Time	14:22:15	14:23:00	14:23:36
Air (cm/s)	3.02	12.21	21.88
Length (mm)	60.42	81.67	110.83

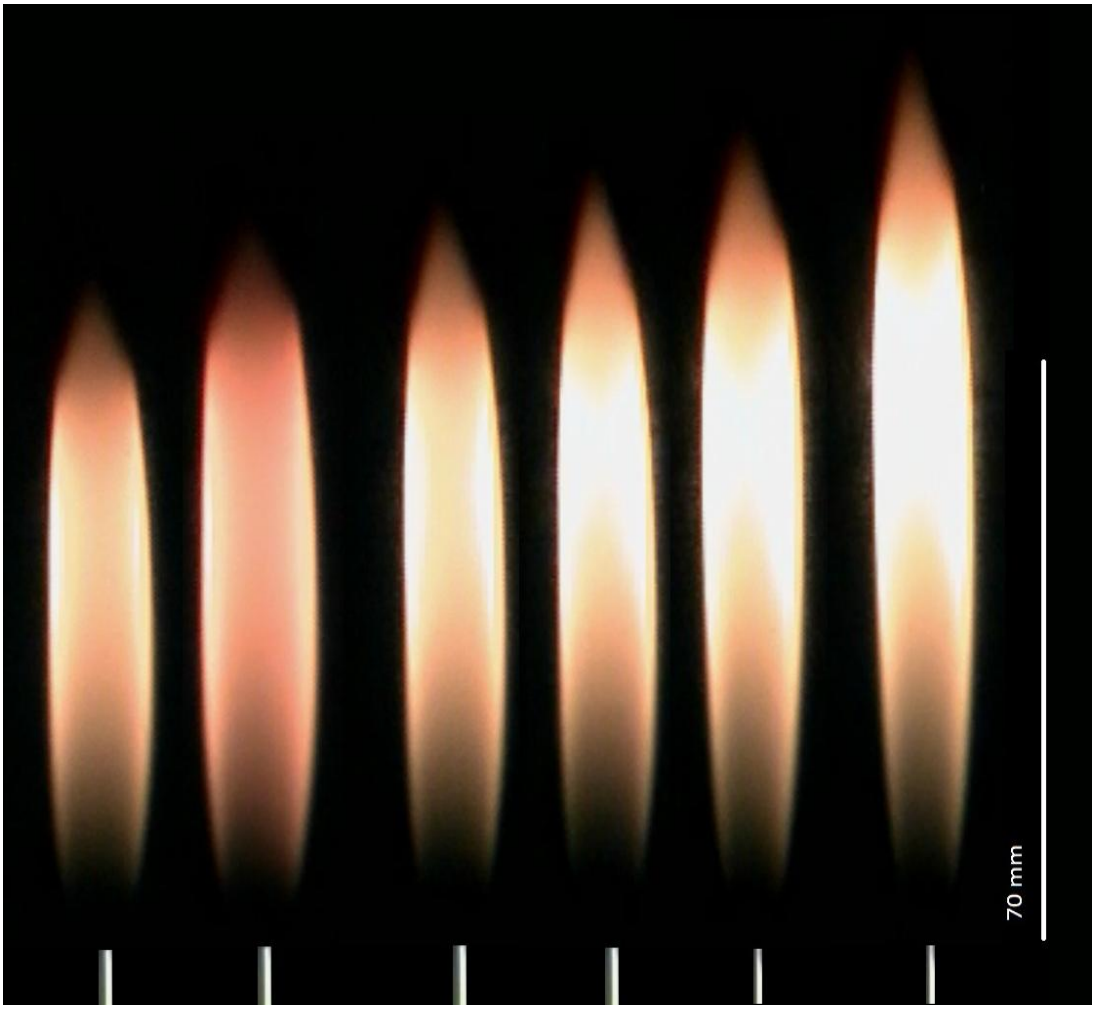

Fuel	CH_4	CH_4	CH_4	CH_4	CH_4	CH_4
Nozzle	3.2	3.2	3.2	3.2	2.1	2.1
GMT	072	072	072	072	072	072
Time	10:46:22	10:46:52	10:47:21	10:48:09	10:58:14	10:58:40
Air (cm/s)	4.2	3.02	8.83	15.51	5.37	6.53
Length (mm)	77.5	75	81.25	85.63	89.17	97.5

References

[1] Turns, Stephen R., *An Introduction to Combustion: Concepts and Applications*. New York: McGraw-Hill, Connect Learn Succeed, 2012. Print.

[2] Betrand, P., "Soot Formation of Lignin Derived Fuels In A Laminar Co-Flow Diffusion Flame." Report Number: WVT2009.09, 2009.

[3] Tien C.L., "Radiation Heat Transfer" *SFPE Handbook of Fire Protection Engineering*, 4th ed., edited by DiNenno, P. J., et al., National Fire Protection Association, Quincy, MA, 2008, pp. 1-73-1-89.

[4] Kennedy, I.M., "The health effects of combustion-generated aerosols," *Proc. Combust. Inst. 31* (2007) 2757–2770.

[5] Purser, D. A., "Assessment of Hazards to Occupants from Smoke, Toxic Gases, and Heat," *SFPE Handbook of Fire Protection Engineering*, 4th ed., edited by DiNenno, P. J., et al., National Fire Protection Association, Quincy, MA, 2008, pp. 2-96-2-193.

[6] Ramanathan, V., and Carmichael, G., "Global and Regional Climate Change Due to Black Carbon," *Nature Geoscience*, Vol. 1, No. 4, 2008, pp. 221-227.

[7] Li, L., Sunderland, P.B., "An Improved Method of Smoke Point Normalization," *Combustion Science and Technology* 184 (2012) 829-841.

[8] Linteris, G. T., and Rafferty, I. P., "Flame Size, Heat Release, and Smoke Points in Materials
Flammability," *Fire Safety Journal*, Vol. 43, No. 6, 2008, pp. 442-450.

[9] Berry, T. L., and Roberts, W. L., "Measurement of Smoke Point in Velocity-Matched Coflow
Laminar Diffusion Flames with Pure Fuels at Elevated Pressures," *Combustion and Flame*, Vol.
145, No. 3, 2006, pp. 571-578.

[10] Dotson, K.T., Sunderland, P.B., "Laminar Smoke Points of Coflowing Flames in Microgravity." *Fire Safety Journal*, Vol. 46, 2011.

[11] Kent, J.H. , Wagner, H.G., "Why do diffusion flames emit smoke?" *Combust. Sci. Technol*. 41 (1984) 245–269.

[12] Glassman, I., "Soot Formation in Combustion Processes," *Twenty-Second Symposium
(International) on Combustion*, The Combustion Institute, Pittsburgh, PA, 1988, pp. 295-311.

[13] Markstein,, G.H., "Relationship between smoke point and radiant emission from buoyant turbulent and laminar diffusion flames," *Proc. Combust. Inst* 20 (1984) 1055–1061.

[14] M.A. Delichatsios, "Smoke yields from turbulent buoyant jet flames," *Fire Saf. J.* 20 (4) (1993) 299–311.

[15] Delichatsios, M.A., "A phenomenological model for smoke-point and soot formation in laminar flames," *Combust. Sci. Technol.* 100 (1994) 283–298.

[16] Roper, F.G., Smith, C., "Soot escape from laminar air-starved hydrocarbon flames," *Combust. Flame* 36 (1979) 125–138.

[17] Markstein, G.H. , "Radiant emission and smoke points for laminar diffusion flames of fuel mixtures," *Proc. Combust. Inst.* 21 (1986) 1107–1114.

[18] D.L. Urban, Z.-G. Yuan, P.B. Sunderland, K.-C. Lin, Z. Dai, G.M. Faeth, "Smoke-point properties of nonbuoyant round laminar jet diffusion flames," *Proc. Combust. Inst.* 28 (2000) 1965–1972.

[19] Roper, F.G. "Soot escape from diffusion flames: a comparison of recent work in this field," *Combust. Sci. Technol*. 40 (1984) 323–329.

[20] Lin, K.-C., Faeth, G.M., Sunderland, P.B. , Urban, D.L., Yuan, Z.-G., "Shapes of nonbuoyant round luminous hydrocarbon/air laminar jet diffusion flames," *Combust. Flame* 116 (1999) 415–431.

[21] Sunderland, P. B., Mortazavi, S., Faeth, G. M., and Urban, D. L., "Laminar Smoke Points of
Nonbuoyant Jet Diffusion Flames," *Combustion and Flame*, Vol. 96, No. 1-2, 1994, pp. 97-103.

[22] Lautenberger, C. W., de Ris, J. L., Dembsey, N. A., Barnett, J. R., and Baum, H. R., "A Simplified Model for Soot Formation and Oxidation in CFD Simulation of Non-Premixed Hydrocarbon Flames," *AIAA Journal*, Vol. 40, No. 2, 2005, pp. 141-176.

[23] Beji, T., Zhang, J. P., and Delichatsios, M., "Determination of Soot Formation Rate from Laminar Smoke Point Measurements," *Combustion Science and Technology*, Vol. 180, No. 5, 2008, pp. 927-940.

[24] Leung, K.M., Lindstedt, R.P., and Jones, W.P. (1991) "A simplified reaction mechanism for
soot formation in nonpremixed flame." *Combust. Flame*, 87, 289.

[25] Moss, J.B., Stewart, C.D., and Young, K.J. (1995) Modeling soot formation and burnout in a high temperature laminar diffusion flame burning under oxygen-enriched conditions.Combust. Flame, 101, 491.

[26] Tolocka, M.P., Miller, J.H. "Production of Polycyclic Aromatic Hydrocarbons fkom Underventilated Hydrocarbon Diffusion Flames" *Chemical and Physical Processes in Combustion.* Fall Technical Meeting, October 16-18, 1995, 253–256 pp, Worcester, MA.

[27] Lin, K.-C., Faeth, G.M., "Hydrodynamic suppression of soot emissions in laminar diffusion flames," *J. Propul. Power* 12 (1) (1996) 10–17.

[28] Urban, D. L., Yuan, Z.-G., Sunderland, P. B., Linteris, G. T., Voss, J. E., Lin, K.-C., Dai, Z., Sun,K., and Faeth, G. M., "Structure and Soot Properties of Nonbuoyant Ethylene/Air Laminar Jet Diffusion Flames," *AIAA Journal*, Vol. 36, No. 8, 1998, pp. 1346-1360.

[29] Glassman, Irvin. *Combustion*. New York: Academic, 2008. Print.

[30] Urban, D. L., Yuan, Z.-Y., Sunderland, P. B., Lin, K.-C., Dai, Z., and Faeth, G. M., "Smoke-Point Properties of Non-Buoyant Round Laminar Jet Diffusion" *Proceedings of the Combustion Institute*, Volume 28, 2000, pp. 1965–1972

[31] Law, C. K., and Faeth, G. M., "Opportunities and Challenges of Combustion in Microgravity" *Prog. Energy Combust. Sci.* 20:65–113 (1994).

[32] Kang, K.T., Hwang, J.Y., Chung, S.H., Lee, W., "Soot zone structure and sooting limit in diffusion flames: comparison of counterflow and co-flow flames." *Combust. Flame 109*, 266–281.

[33] Sivathanu, Y. R., and Faeth, G. M., "Temperature / Soot Volume Fraction Correlations in the Fuel-Rich Region of Buoyant Turbulent Diffusion Flames," *Combustion and Flame*, Vol. 81, No. 2, 1990, pp. 133-149.

[34] Santoro, R. J., Yeh, T. T., Horvath, J. J., and Semerjian, H. G., "The Transport and Growth of Soot Particles in Laminar Diffusion Flames," *Combustion Science and Technology*, Vol. 53, No. 2, 1987, pp. 89-115.

[35] Lin, K.-C. and Faeth, G. M., "Shapes of Nonbuoyant Round Luminous Laminar-Jet Diffusion Flames in Coflowing Air," *AIAA Journal*, Vol. 37, No. 6, 1999, pp. 750-765.

[36] Schalla, R. L. and McDonald, G. E., "Mechanism of Soot Formation in Flames," *Fifth Symposium (International) on Combustion*, The Combustion Institute, Pittsburgh, PA, 1955.

[38] Dotson, K.T., Sunderland, P.B. "Laminar Smoke Points of Coflowing Flames in Microgravity." *University of Maryland*, 2009.

[39] Berry Yelverton, T. L., Roberts, W. L., "Effect of Dilution, Pressure, and Velocity on Smoke Point in Laminar Jet Flames," *Combustion Science and Technology*, Vol. 180, No. 7, 2008, pp. 1334-1346.

[40] Schalla, R. L., Hibbard, R. R.: "'Smoke and Coke Formation in Combustion of Hydrocarbon-Air Mixtures," Chap. IX in *NACA Repor*t 1300, 1959.

[41] Venkat, C., Brezinsky, K., Glassman, I.: *Nineteenth Symposium (International) on*

Combustion, p. 143, The Combustion Institute,1982.

[42] Benson, S. W.: *Twenty-First Symposium (International) on Combustion*, p. 703, The Combustion Institute, 1988.

[43] Frenklach, M.: "'On The Driving Force of PAH Production," *Twenty-Second Symposium*
(International) on Combustion The Combustion Institute, Pittsburgh, PA, 1988.

[44] Santoro, R. J., Semerjian, H. G., and Dobbins, R. A., "Soot Particle Measurements in Diffusion Flames," *Combustion and Flame*, Vol. 51, 1983, pp. 203-218.